ELSEVIER

Earth-Science Reviews 39 (1995) 169–206

EARTH-SCIENCE REVIEWS

Cloud venting — A review and some new global annual estimates

W.R. Cotton *, G.D. Alexander, R. Hertenstein, R.L. Walko, R.L. McAnelly, M. Nicholls

Colorado State University, Dep. of Atmospheric Science, Fort Collins, CO 80523, USA

Received 16 February 1994; accepted 16 January 1995

Abstract

In this paper we review observational and modeling studies of cloud venting by a wide variety of cloud types ranging from ordinary cumuli, to ordinary cumulonimbi, mesoscale convective systems and tropical and extratropical cyclones. We have used explicit cloud-resolving simulations with RAMS to illustrate the nature of the process of venting of boundary layer air by several cloud system types and to provide quantitative estimates of the transport rates for different storms.

In order to help global modelers prioritize their efforts in developing and refining cloud transport parameterization schemes, we have also attempted to make global estimates of the contributions of the various storm types to venting of boundary layer air. We find that on a global-annual basis, the extratropical cyclone has the highest boundary layer mass flux of all cloud venting systems, followed by the general class of MCS's (excluding MCC's), ordinary thunderstorms, tropical cyclones, and MCC's. We estimate an annual flux of 4.95×10^{19} kg of boundary layer air by these cloud systems, which represents a venting of the entire boundary layer about 90 times a year.

1. Introduction

The term "cloud venting" refers to the process of transporting gaseous matter and aerosol (including pollutants) from the lower troposphere into the cloud layer (i.e., the middle and upper troposphere) (Ching, 1982). Many aerosol particles are readily scavenged by cloud droplets during nucleation (nucleation scavenging) or are collected by falling hydrometeors, and thereby subjected to aqueous-phase chemical reactions. Moreover, many gases are absorbed on the surface of droplets and can also undergo aqueous-phase chemical reactions. The ultimate fate of these species is thus determined by the chemical composition of the species, the air motions of the clouds and their immediate environment, and by the extent they become involved in the precipitation process of a cloud or cloud system.

We begin this review with an introduction to the theoretical foundations of the problem. We then discuss the research that has been done in observing and modeling cloud venting involving boundary layer clouds, deep convective clouds,

* Corresponding author.

SSDI 0012-8252(95)00007-0

mesoscale convective systems, and clouds embedded in extratropical cyclones. In the spirit of the GEWEX Cloud Systems Study (GCSS) program (see Browning, 1993), throughout this review we use cloud-resolving simulations of convective clouds and mesoscale convective systems that have been performed by our group using the Regional Atmospheric Modeling System (RAMS) developed at Colorado State University (see Tripoli and Cotton, 1989a,b; Cram et al., 1992a,b; Pielke et al., 1992; Walko et al., 1992) to provide quantitative estimates of cloud venting rates. In order to help global modelers prioritize their efforts in developing and refining cloud transport parameterization schemes, we conclude with some global estimates of cloud venting by clouds of various types.

2. Theoretical foundations

2.1. Equations for mixing ratios of species in air

To describe the venting or transport of a pollutant having a mixing ratio C_i, a conservation equation of the form:

$$\frac{\partial C_i}{\partial t} + \vec{V} \cdot \nabla C_i = \nu \nabla^2 C_i + R_i + S_i - G_i^j \qquad (1)$$

can be written. $\vec{V}$ is the three-dimensional velocity vector, ν is the kinematic viscosity of air, R_i is a chemical reaction term, S_i is a source term or sink term, and G_i^j describes the transfer rate of the ith species between the gas phase and the jth hydrometeor species. The first term on the left hand side (LHS) of Eq. (1) represents the local (at a fixed point in space) time rate of change of the mixing ratio of the pollutant. The second term on the LHS represents the transport or advection of C_i. The first term on the right hand side (RHS) represents the molecular diffusion of C_i. In Eq. (1) it is assumed that the pollutant has negligible fall velocity through the air. This assumption is valid for gases and small (sub-micrometer) aerosol particles. For faster settling species, a sedimentation term must be added to Eq. (1). Strictly speaking Eq. (1) is only valid for infinitely small volumes of air. Most models of cloud venting require averaging over finite volumes, or over an ensemble of turbulent eddies. As a result, the classical Reynolds averaging procedure is invoked which transforms Eq. (1) into an equation for the average mixing ratio of the pollutant. To do so, we decompose the variables in Eq. (1) into mean and fluctuating components:

$$C_i\left(\underset{\sim}{x},t\right) = \overline{C}_i\left(\underset{\sim}{x},t\right) + C_i'\left(\underset{\sim}{x},t\right)$$

$$\vec{V} = \overline{\vec{V}} + \vec{V}'$$

$$R_i = \overline{R}_i + R_i' \qquad (2)$$

$$S_i = \overline{S}_i + S_i'$$

$$G_i^j = \overline{G_i^j} + G_i'^j.$$

Assuming that the turbulence behaves as an incompressible fluid and ignoring correlations between fluctuating and mean variables (see Cotton and Anthes (1989) for a detailed description of the Reynolds averaging procedure), the time rate of change of the average mixing ratio C_i is:

$$\frac{\partial \overline{C}_i}{\partial t} + \vec{V} \cdot \nabla \overline{C}_i = \nabla \cdot \overline{\vec{V}' C_i'} + \overline{R}_i + \overline{S}_i - \overline{G_i^j}. \qquad (3)$$

In Eq. (3), we have ignored molecular diffusion since it is much smaller in magnitude than the turbulent diffusion term (first term on the RHS of Eq. 3). The turbulent diffusion term requires the use of a closure model. For large eddy simulation (LES) or cloud-resolving models, the turbulent transport term is parameterized using a sub-grid-scale closure model. Normally this is an eddy diffusion model in which turbulence is parameterized in analogy to molecular diffusion, except that a much larger eddy viscosity replaces the kinematic viscosity of Eq. (1). Alternately, the turbulent diffusion term can be modeled by using higher order closure theory in which prognostic equations on turbulent covariances and variances are formulated (see Cotton and Anthes, 1989). The addition of these equations greatly increases the computational expense of a cloud venting model. In larger scale models which cannot explicitly resolve the dominant energy-containing eddies in the atmospheric boundary layer

(ABL) or the cloud layer, $\overline{C}_i$ represents the ensemble-average mixing ratio of our pollutant rather than the grid-scale average. The distinction is that an ensemble-average turbulence model is supposed to represent transport by all turbulent eddies, whereas a sub-grid-scale turbulence closure model represents transport only by eddies smaller than some arbitrary length (normally the grid scale of the model). In its application to larger-scale models the ensemble-average closure model need not have any dependence on the horizontal grid spacing of the host model. Moreover, the ensemble-averaged turbulence model represents the average of a large number of realizations under meteorologically look-alike conditions (see Cotton and Anthes, 1989). For very large scale models, such as general circulation models and regional transport models, further simplifications to Eq. (3) can be justified. First of all, we can assume that horizontal turbulent fluxes are small compared to vertical fluxes. Then Eq. (3) becomes:

$$\frac{\partial \overline{C}_i}{\partial t} + \overrightarrow{\overline{V}} \cdot \nabla \overline{C}_i = -\frac{\partial}{\partial z}\left(\overline{w'C_i'}\right) + \overline{R}_i + \overline{S}_i - \overline{G_i^j}. \quad (4)$$

Furthermore, it is generally recognized that a down-gradient eddy diffusion model is an inadequate description of vertical transport by cumulus clouds (e.g. Chatfield and Crutzen, 1984). An eddy diffusion model slowly mixes highly concentrated pollutants from the boundary layer upwards, producing a relatively uniform concentration through the depth of the troposphere. Cumulus clouds, on the other hand, sweep vast quantities of pollutants from the boundary layer and inject them into the upper troposphere in a few tens of minutes. This often produces high concentrations of pollutants at detrainment levels with little material through the remainder of the troposphere. Therefore, when dealing with cumulus cloud transport in larger scale models, it is common to modify the Reynolds averaging procedure into a "tophat" averaging scheme in which cloud transports are separated from environmental transports (e.g., Cho et al., 1983). Using a subscript c to denote properties of air inside cumulus clouds, and a tilde to denote air properties in the cloud environment, the average C_i can be expressed as

$$\overline{C}_i = \sigma C_{ic} + (1-\sigma)\tilde{C}_i. \quad (5)$$

Here σ represents the fractional areal coverage occupied by clouds. The cloud vertical eddy flux is then given by

$$\overline{w'C_i'} = \sigma(1-\sigma)\left(w_c - \tilde{w}\right)\left(C_{ic} - \tilde{C}_i\right). \quad (6)$$

As shown by Cho et al. (1983), if we assume that $|w_c| \gg |\tilde{w}|$ and that $\overline{C}_i \approx \tilde{C}_i$ then

$$\overline{w'C_i'} = -M_c\left(C_{ic} - \overline{C}_i\right). \quad (7)$$

where M_c is the so-called cloud mass flux defined as

$$M_c = +\sigma w_c. \quad (8)$$

Eq. (7) shows that the vertical eddy flux of a pollutant is proportional to the difference in pollutant mixing ratios between clouds and their environment.

2.2. Equations for species embedded in hydrometeors

The above equations are valid for a pollutant that is in cloud-free air or is interstitial in cloudy air. Following notation by Kitada et al. (1993), the continuity equation for the mixing ratio (defined relative to the mass of a hydrometeor) of pollutants embedded in hydrometeors is

$$\frac{\partial \overline{C_i^j r_j}}{\partial t} + \overrightarrow{\overline{V}_j} \cdot \nabla \overline{C_i^j r_j} - \overline{V}_j \frac{\partial \overline{C_i^j r_j}}{\partial z} - \overline{r}_j \frac{\partial\left(\overline{V_j C_i^j}\right)}{\partial z}$$

$$= \nabla \cdot \overrightarrow{\overline{C_i^j V' x'}} + \left(\overline{R_j^i} + {}_k\overline{T_i^j} + \overline{G_i^j}\right). \quad (9)$$

Here C_i^j, represents the mixing ratio of the ith chemical species embedded in the jth hydrometeor species having mixing ratios r_j, V_j represents the terminal fall speed of the jth hydrometeor species, R_j^i represents the reaction term of the ith species in the jth hydrometeor class, ${}_kT_i^j$ denotes the transfer rate of the ith species from the jth hydrometeor to the kth hydrometeor, and G_i^j is the same as in Eq. (1). Examples of hydrometeor classes would be cloud droplets, rain-

drops, ice crystals, aggregates, graupel and hail. The added complication of Eq. (9) relative to Eq. (3), is that we must keep track of the concentration of the species in the individual hydrometeors as well as the concentrations of the hydrometeors. We must also consider the effects of the sedimentation of the hydrometeors, as well as the special aqueous-phase chemical reactions. As one can readily see, keeping track of pollutants or chemical species in hydrometeors while undergoing chemical reactions and transferring from one hydrometeor class to another is a complicated bookkeeping problem.

3. Ordinary cumuli

By ordinary cumulus clouds, we mean either cumulus clouds that are confined by a capping inversion (such as fair weather cumuli or cumulus humilis), or lightly-precipitating towering cumuli. These clouds form from buoyant thermals of air that develop in the atmospheric boundary layer (ABL). The thermals derive their energy from solar heating of the Earth's surface, or from heat and moisture fluxes from the ocean surface. Fig. 1 illustrates a typical temperature and dew point sounding that supports ordinary cumulus clouds. The sounding is unstable to dry air motions near the Earth's surface and nearly neutral up to the top of the ABL labeled Z_i. The shallow layer just above Z_i is stable to dry motions. In the ABL a variety of thermals form. Some are small and only weakly buoyant, while others may be larger and more buoyant. As the thermals rise and cool adiabatically, they mix with non-buoyant air in the ABL, thus losing their buoyancy. A few thermals may be buoyant enough to rise to the lifting condensation level (LCL) where they become saturated and a cloud forms. Those that rise slightly above the LCL and lose their buoyancy are referred to by Stull (1985) as "forced cumuli" (see Fig. 1). They are only able to transport (vent) boundary layer material a short distance above Z_i. Other, more buoyant thermals, may ascend to the level of free convection (LFC) where latent heat liberated during condensation to form droplets yields enough buoyancy for the cloud to ascend into the capping inversion. Stull (1985) referred to such clouds as "active cumuli". Such clouds can transport ABL air to greater heights and provide an aqueous environment for sustained chemical reactions. Upon encountering the capping inversion, the cloud quickly loses its buoyancy. Dry air is mixed into the cloud interior further eroding the cloud buoyancy. The residue left by the now non-buoyant cloud is what Stull (1985) referred to as a "passive cloud" (see Fig. 1). This cloud slowly evaporates leaving behind the debris of material it has vented from the ABL

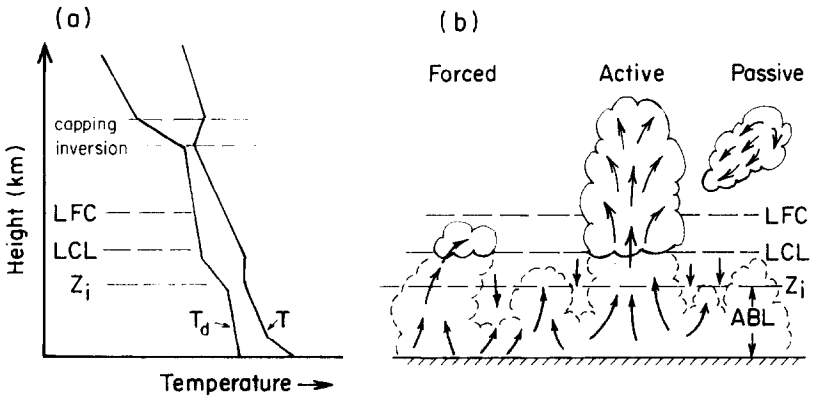

Fig. 1. (a) Atmospheric sounding in which fair weather cumulus clouds prevail. Indicated is the air temperature T, the dewpoint temperature T_d, the height of the atmospheric boundary layer Z_i, the lifting condensation level (LCL), the level of free convection (LFC) and the capping temperature inversion. (b) Illustration of forced cumuli, active cumuli and passive cumuli. (Adapted from Stull, 1985).

during its active period. The debris may have undergone chemical reactions during the cloud lifetime. Furthermore, as the droplets evaporate, they often leave behind aerosol particles which are larger than the initial cloud-forming aerosol particles and chemically altered as well (Hoppel et al., 1986; Mitra et al., 1992).

Observations of ordinary cumulus cloud venting have been made with in situ aircraft measurements (Isaac et al., 1983; Ching and Alkezweeny, 1986; Greenhut, 1986), and with airborne remote sensing platforms such as a UV-DIAL (ultraviolet differential absorption lidar). Isaac et al. (1983) defined the cloud transport ratio (VTR) as the volume of sub-cloud air that is pumped through the base of cumuli on an hourly basis divided by the volume of the sub-cloud air. That is,

$$VTR = \frac{wA_{CL}F}{(HA_{\mathrm{TOT}})}, \tag{10}$$

where w is the updraft velocity at cloud base, H is the height of cloud base above ground, F is the hourly frequency of observation, A_{CL} is the total cross-sectional area of the cloud bases and A_{TOT} is the total area of the region. For summer cumuli over Ontario, Canada, Isaac et al. found VTR values of about 20% per hour, while those for stratocumuli were somewhat less. Thus, in spite of their small coverage relative to stratocumuli, cumulus clouds pump as much or more air through their bases. Averaging over all cloud types, they found that in the summer, about 50% of the sub-cloud air is vented through cloud base on an hourly basis. Winter values were less — approximately 20%.

In the southeast United States, Ching et al. (1988) used a UV-DIAL system to measure O_3 profiles in the lower troposphere. This system can measure the time-integrated products of convective injections of O_3 and aerosol in the atmosphere. In one case they found enhanced concentrations of O_3 at levels well above the ABL. This was attributed to deep convective injection of power plant plume material upwind of the Lidar.

Greenhut (1986) reported on the analysis of fast response measurements of O_3 and w with an aircraft flying through the cloud layer and sub-cloud layer. He found that the vertical O_3 flux could be described by the simple formula

$$\overline{w'O_3'} = -\overline{w}\Delta O_3, \tag{11}$$

where ΔO_3 is the difference in concentration between the cloud layer and the ABL, and $\overline{w}$ is the cloud layer vertical velocity averaged over the time of observation. Eq. (11) is similar in form to Eq. (7), but the terms are different.

Ching and Alkezweeny (1986) released inert tracers (SF_6) beneath actively rising cumulus clouds and in the cloud layer. They found that some of the tracers released beneath cumulus clouds were entrained in the cumulus updrafts and then ascended relatively undiluted into the cloud layer. Tracers released within the cloud layer, however, experienced rapid descent within the cloud-free air between the clouds, entered the ABL, and some even reached the surface. They estimated that downdrafts of the order of 1.5 ms^{-1} had to be present to account for the rapid descent of the tracer. Such values are considerably larger than one would expect for synoptic-scale subsidence (or even compensating subsidence for the cloud updrafts), assuming that the subsidence is uniformly distributed over the cloud-free portion of the cloud layer.

The approaches to modeling of venting by ordinary cumuli range from use of sophisticated two- and three-dimensional numerical prediction cloud models with either bulk microphysics or explicit bin-resolving microphysics to simpler one-dimensional cloud models. We discuss examples of each, in turn, below.

One of the most sophisticated models of cloud venting is the two-dimensional numerical prediction model with explicit, bin-resolving microphysics described by Flossman (1991,1993) and Flossman and Pruppacher (1988). The basic dynamic framework of the model is a two-dimensional slab based on the two- and three-dimensional cloud model described by Clark (1977,1979), Hall (1980), and Clark and Farley (1984). The equations of motion, thermodynamic energy, water components and aerosol conservation, are solved on a finite difference grid. Flossman and Pruppacher (1988) added conservation equations for the number and mass density distri-

bution functions for ammonium sulfate and sodium chloride particles in air, and the mass density function for ammonium sulfate and sodium chloride particles in drops to the Hall (1980) model containing conservation equations for cloud droplet number density function. In all, 57 bins describe the evolution of cloud microstructure along with 81 additional bins to describe the aerosol physics and chemistry at each grid point. This model explicitly considers the changes in the cloud droplet spectra caused by condensation and evaporation, collision and coalescence of drops, drop breakup, nucleation and impaction scavenging of aerosol, and oxidation inside drops that have been nucleated on aerosol. Because it is limited to two-dimensions, this model will underestimate the entrainment of pollutants in the sub-cloud air in active updrafts and the dilution of the pollutants in the cloud layer by entrainment of clean environmental air, relative to a three-dimensional model. The two-dimensional framework is, nonetheless, computationally economical and is, therefore, useful in gaining experience in performing calculations with a complex model in which the physics and chemistry of the droplet and aerosol spectra are calculated numerically at each grid point. Transport and diffusion are then calculated numerically on the two-dimensional finite difference grid. The model has demonstrated that in-cloud scavenging of hygroscopic aerosol particles is mainly controlled by nucleation scavenging or the scavenging of hygroscopic particles as they become activated as cloud droplets. Impaction scavenging, or removal by the collection of aerosol by hydrometeors, on the other hand, played a negligible role (Flossman, 1991). Subcloud impaction scavenging contributed only 5% to overall particle scavenging. However, it contributed about 40% of the aerosol mass since mainly larger particles are scavenged there. Likewise, the model demonstrated that the scavenging efficiency of a cloud is closely related to the precipitation efficiency (defined as the rainfall rate divided by the flux of water vapor entering cloud base) of the cloud. In fact, Flossman (1993) concluded that for simulations of average clouds at a given location, a detailed knowledge of impaction efficiency is not necessary. Only if it is desired to know how the pollutants are distributed across the droplet spectra, is it important to calculate the details of the scavenging process. In that case, it is important to know the initial vertical distribution of pollutants to determine the effects of subcloud scavenging on the distribution of pollutants on the drops.

Kitada et al. (1993) developed a two-dimensional/three-dimensional cloud model with mixed-phase bulk microphysics, aqueous-phase chemistry, and dry and wet depositional processes. They accounted for six aqueous species: NO_3^-, NH_4^+, S(IV), SO_4^{2-}, H_2O_2 and O_3. Application of their model to snow-producing cumuli over the Sea of Japan (Kitada and Lee, 1993) revealed that the complex cycle of absorption and nucleation scavenging of gases and aerosol in the cloud layer, followed by transfer of the chemical species to snow by ice particle riming, and finally the sedimentation and release of the aerosol and gases in the subcloud layer by sublimating snow crystals, maintains higher subcloud concentrations of the gases and aerosol than in cloud-free situations. This is an example of cloud "trapping" rather than "venting".

An example of the application of a three-dimensional numerical prediction model to cloud venting by fair weather cumuli using RAMS is as follows. RAMS was initialized with a horizontally homogeneous sounding obtained as part of the BLX83 experiment (Stull and Eloranta, 1984) on 7 June 1983. The sounding exhibited a strong capping inversion at 2700 m and weak to moderate stability below the inversion. Wind speeds ranged from zero to around 20 m s^{-1} at and below the inversion. The first fair weather cumuli were observed about 1100 local time. RAMS was set up as a large eddy simulation (LES) model over a 6 km × 6 km horizontal domain with cyclic boundary conditions. The vertical depth of the model domain was 4.7 km, and 100 m grid spacing was used in all directions. The initial water vapor field was moistened somewhat at low levels compared to the sounding because of the uncertainties in surface transpiration and evaporation.

The model simulated the development of a convective boundary layer over a solar-heated ground, eventually producing cumuli. At local

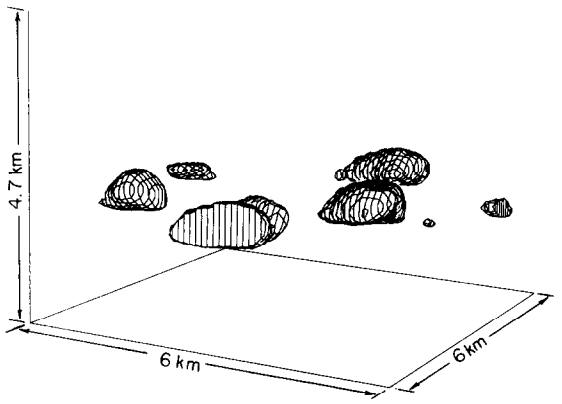

Fig. 2. Three-dimensional depiction of cumulus clouds at local noon as viewed from the southeast.

noon the simulated clouds (see Fig. 2) had a coverage of about 30% and had bases of about 1500 m, or ~ 300 m lower than observed. At this time, a total of 100,000 Lagrangian particle tracers were released uniformly throughout the lowest 1500 m of the domain. The cumuli carried many of the particles upwards towards the inversion or slightly above. A time series of average particle concentrations is shown in Fig. 3. Also shown in the figure are the cloud base and inversion heights during the period. These fair weather cumuli transport over 30% of the boundary layer air over the 36 km^2 area above their bases in one hour, but little is transported above the capping inversion. As compared to the deep convective clouds discussed later, the fair weather cumuli are not major venters of boundary layer air, but instead tend to enhance vertical mixing in the boundary layer, as stated, for instance, by Riehl (1979) and Riehl and Malkus (1958).

An example of the application of a three-dimensional numerical prediction model to cloud venting of towering cumuli is the use by Tremblay and Leighton (1986) of the three dimensional cloud model of Yau (1980). Starting with the single-cloud model of Yau and Michaud (1982), they introduced continuity equations for chemistry of SO_2, HNO_3, NH_3, H_2 O_2, O_3, CO_2, and sulfate aerosol including rainout and washout. The model was initialized with a sounding of temperature, moisture, winds, and aircraft observations of clear air chemistry taken at North Bay, Ontario, Canada during a field study in July 1982 (see Isaac et al., 1982; Leaitch et al., 1982). Averaging over the model domain, Tremblay and Leighton calculated that 1% of the SO_2 below 1 km was vented into upper levels by the single cloud during its lifetime. Using the observed spacing of cumuli, for the case studied, yields an average transport of SO_2 across the 2 km level of about 4% per hour. Budget calculations of simulated nitrate and sulfate species indicated that 60–70% of the mass of the species deposited at the surface in rain is generated by in-cloud processes, while the remainder is scavenged in the subcloud layer.

Simulation of venting by a field of towering cumuli near Miles City, Montana has been accomplished by Niewiadomski (1986) who introduced passive tracers into the model of Smolarkiewicz and Clark (1985). Starting from a horizontally-homogeneous initial sounding, they simulated the development of a field of non-precipitating towering cumuli in response to local terrain forcing (see Fig. 4). The initial profile of the

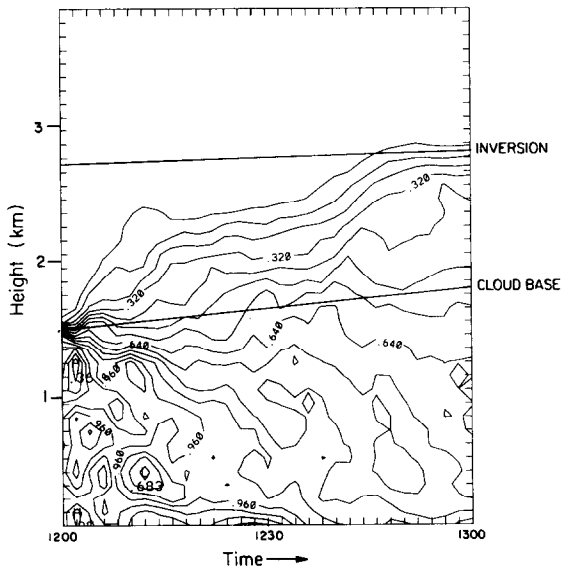

Fig. 3. Horizontally-averaged tracer concentration profile as a function of time. Added lines show the height of the cloud base and inversion as a function of time. Values are normalized to the initial boundary layer concentration of 1.0.

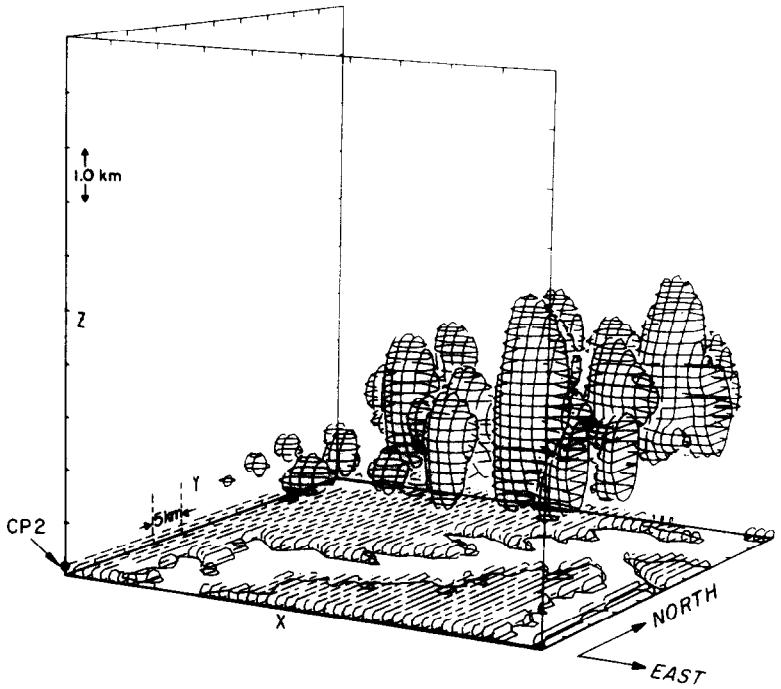

Fig. 4. An example of the "numerical" clouds where the surfaces of $q_c = 0.1$ g kg^{-1} are shown in a perspective plot. The full model domain of $50 \times 50 \times 10$ km in the x, y and z directions is shown (from Smolarkeiewicz and Clark, 1985).

pollutant exhibited a maximum at ~ 0.7 km AGL (Fig. 5). The pollutant, shown in Fig. 6, was vented from the ABL to heights ranging from 2.5 to 6.5 km. It was noted that in active cores of the cumuli, concentrations of the pollutant remained high with little indication of any dilution by entrainment. Niewiadomski (1986) calculated that these clouds reduced concentrations of the pollutant in the boundary layer by 15% over a one hour average. Likewise, he calculated that the average VTR was about 23% per hour for this case.

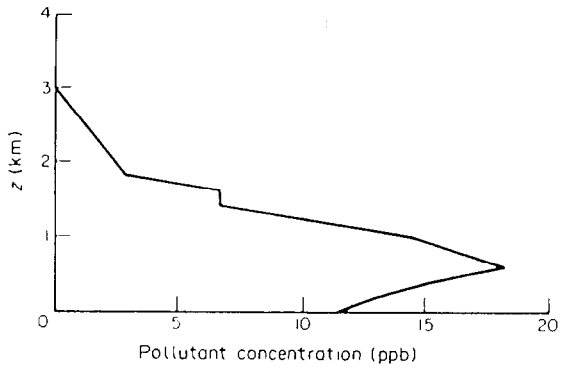

Fig. 5. Assumed profile of the pollutant imposed as the initial condition at 8:00 a.m. (From Niewiadomski, 1986. Reprinted from *Atmospheric Environment* with kind permission from Pergamon Press Ltd., Headington Hill Hall, Oxford OX3 0BW, UK, see reference list for full citation.)

In addition to the more complex cloud models described above, a number of investigators have used simplified one-dimensional models that can be used in regional long-range pollutant transport models or even general circulation models. Some examples of these are Walcek and Taylor (1986), Ching (1989) and Vukovich and Ching (1990). Walcek and Taylor (1986) used a one-dimensional plume model in which the vertical profile of cloud liquid water content was adjusted to match the observed profile of liquid water relative to adiabatic (unmixed) liquid water reported by Warner (1970). This was interpreted to represent the effects of cloud top entrainment. It was

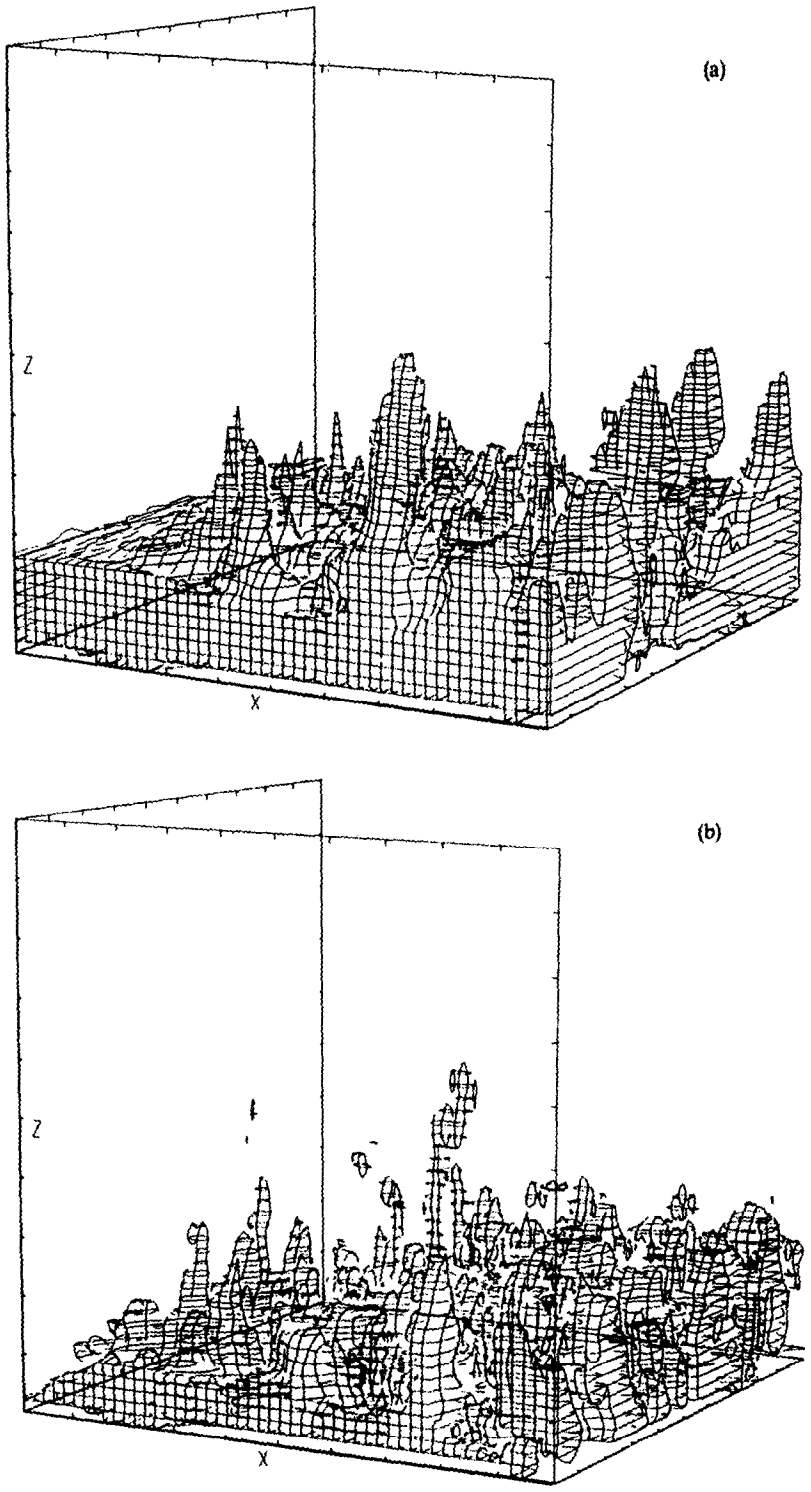

Fig. 6. Isosurface of 7 ppb pollutant concentration at 10:00 a.m. (a), and 11:00 (b). (From Niewiadomski, 1986. Reprinted from *Atmospheric Environment* with kind permission from Pergamon Press Ltd., Headington Hill Hall, Oxford OX3 0BW, UK, see reference list for full citation.)

noted in Niewiadomski's (1986) three-dimensional simulation, however, that the cores of the convective towers remained unmixed. This is inconsistent with Warner's (1970) observational analyses. Nonetheless, there are observations which suggest that the cores of convective towers remain largely unmixed (e.g., Heymsfield et al., 1978), allowing higher concentrations of pollutants to be transported aloft than with Walcek and Taylor's model.

One of the advantages of a one-dimensional modeling framework is that atmospheric chemistry can be introduced rather simply. Walcek and Taylor introduced an aqueous chemistry model in their cloud plume model and calculated vertical variations in pH, among other things. They found that the pH generally increased with height above cloud base, primarily caused by the dilution of the dissolved sulfate aerosol. They also found that factors such as temperature, pressure, degree of entrainment and liquid water content variations all affected the vertical variations in cloud chemical composition.

Several investigators have extended the one-dimensional model framework to two or three axisymmetric cylinders that surround a central core updraft (Lee, 1986; Niewiadomski et al., 1986; Cho et al., 1989; Taylor, 1989a,b). This modeling framework is an extension of the original Asai and Kasahara (1967) cloud model. In this approach, sometimes referred to as a 1.5D model, cloud dynamics, microphysics and chemistry are calculated by numerical prediction techniques for a one-dimensional column for each of the axisymmetric cylinders that are employed in the model. The model is time-dependent, thus simulating the evolution of a single cloud through initiation and maturity, to decay. The advantage of this approach is that it is still sufficiently simple that rather complex chemistry models can be added and that the time evolution of cloud updrafts and downdrafts and their associated microphysics and chemistry can be simulated. The models suffer from the inability to simulate the effects of shear or multiple-cloud interactions. Moreover, they are dominated by lateral entrainment, which numerous investigations have shown is an inadequate representation of bulk cloud mixing processes (e.g., Warner, 1970; Cotton, 1975; Paluch, 1979; Boatman and Auer, 1983; Blyth and Latham, 1985; Jensen et al., 1985).

We will see that simple one-dimensional cloud models are also used to calculate cloud venting and cloud chemistry in thunderstorms and extratropical storms as well.

4. Venting by cumulonimbus clouds

Cumulonimbus clouds are rain-producing, deep tropospheric clouds generally accompanied by lightning, thunder and gusty surface winds. The characteristics of cumulonimbus clouds vary depending upon the environmental thermodynamic and wind structure through the troposphere. Two parameters reasonably well define the regimes for different cumulonimbus types. One is the convective available potential energy (CAPE). CAPE is the positive energy available to a parcel of air ascending from the surface to the top of a cloud, or where the cloud temperature equals the environmental temperature,

$$\mathrm{CAPE} = g\int \frac{\theta_m(z) - \bar{\theta}(z)}{\bar{\theta}(z)}\,dz, \tag{12}$$

where $\theta_m(z)$ is the potential temperature of a rising parcel ascending moist adiabatically, and $\bar{\theta}(z)$ is the potential temperature of the environment. CAPE represents the energy associated with the positive area on a skew-T, log-P thermodynamic diagram. The other parameter is the bulk Richardson number which has been defined by Moncrieff and Green (1972) as

$$R_i = \frac{\mathrm{CAPE}}{1/2(\Delta u)^2} \tag{13}$$

where Δu represents the vector shear magnitude between low levels and middle levels of the troposphere, or between the level of free convection (LFC) and the level of neutral buoyancy.

In environments with relatively modest values of CAPE (CAPE < 2000 joules/kg) and large values of R_i ($R_i > 50$), ordinary thunderstorms are likely. Such thunderstorms have a lifetime of approximately one hour and go through a character-

istic lifecycle of growth, maturity, and decay (see Cotton and Anthes, 1989) within that time.

Ordinary thunderstorms typically have peak updraft strengths of approximately 8 to 15 m s^{-1} exhibit moderate lightning frequencies ($\sim$ 2 to 3 flashes per minute) and produce rainfall amounts over their lifetime of usually less than 25 mm (occasionally over 50 mm). Precipitation efficiencies are generally quite variable, with one report (Braham, 1952) being as low as 10%. Ordinary thunderstorms are common in the tropics and sub-tropics.

In environments where CAPE is large (> 3000 joules/kg), but $R_i > 50$, intense multicellular storms are likely (Weisman and Klemp, 1984). These storms are composed of a number of thunderstorm cells that resemble ordinary thunderstorms. Some cells are in growth, some in mature, and others in dissipating stages. Peak updrafts in the cells can often exceed 35 m/s, and they can produce large hail, heavy rains (as large as 250 mm over their lifetime), and strong surface winds including tornadoes. Precipitation efficiencies in severe multicell storms have been observed to be quite high, exceeding 80% (Marwitz, 1972a,b,c). Owing to the large number of cells, multicellular thunderstorms often exhibit frequencies of lightning as high as 35 flashes per minute (Pakiam and Maybank, 1975). The lifetime of multicellular severe storms is typically between two and six hours.

In environments with values of CAPE > 3000 joules/kg and in which $15 < R_i < 35$, supercell thunderstorms are likely. These storm systems are characterized by a dominant, steady, rotating single cell with peak updraft strengths that can exceed 40 m s^{-1}. Precipitation efficiencies are often quite low, with values of 20% being common (Marwitz, 1972a,b,c). Owing to the strong upward flux of moisture in supercells, however, they can still process large amounts of water and contribute to localized flash flooding. Supercells have lifetimes that can exceed six hours, but generally move quite rapidly. In some cases the lightning frequency in supercells is only 2–3 flashes per hour which has been interpreted to be related to its unicellular character (Pakiam and Maybank, 1975). However, supercells with higher lightning frequencies are possible. Supercells are notorious for producing tornadoes, giant hail and severe winds. Although their frequency is low, they can transport large amounts of pollutants aloft owing to their large updraft strengths, relatively low precipitation efficiencies, and long lifetimes.

As can be seen from the above, there is quite a range of cloud transport characteristics depending on the particular mode of convection. One would expect, then, regional differences in cloud transport properties since environmental properties such as CAPE and vertical shear of the horizontal wind vary in a climatological sense regionally. For example, deep tropospheric shear is typically weaker in the tropics than at higher latitudes. CAPE, likewise, is less over the tropical oceans than in the central U.S. during the summertime. CAPE, however, can be quite large over continental areas of the tropics during undisturbed periods (Williams et al., 1992). Chatfield et al. (1987), for example, found it necessary to adjust their parameterized cloud transport model when it was moved from tropical environments to middle latitudes. Some of the adjustments may have been due to differing modes of convection, but their scheme includes the coverage of cumulonimbi. As they noted, the frequencies of cumulonimbi are generally higher in the tropics than in mid-latitudes. The particular mode of convection can also be important to the chemistry of cumulonimbi because, as noted above, the precipitation efficiency (which impacts the efficiency of removal of aerosols and gases) varies from ordinary thunderstorms to supercell storms. Moreover, electrical generation of gases (e.g., NO_x) and particulates should vary with storm type since the frequency of lightning activity appears to vary with the mode of convection.

There have been only a few direct observations of venting by cumulonimbus clouds. Dickerson et al. (1987) described the analysis of a multicellular thunderstorm that occurred during the 1985 Preliminary Regional Experiment for STORM-Central (PRESTORM) (see Cunning, 1986) and the Processing of Emissions by Clouds and Precipitation (PRECP) in the Oklahoma–Kansas region of the United States. Aircraft equipped with

air and precipitation chemistry sensors, as well as meteorological sensors, penetrated the storm at multiple levels. The primary tracers used to investigate cloud venting were CO and, to a lesser extent, O_3. CO is primarily produced at the Earth's surface and destroyed throughout the troposphere so that it generally decreases with altitude. O_3, on the other hand, is produced primarily in the stratosphere and is destroyed at the earth's surface and increases with altitude. Based on the CO analysis, Dickerson et al. estimated that the anvil of the storm was composed of about 64% ABL air and 36% upper tropospheric air and found that ozone exhibited a local maximum in the anvil. They speculated that the source may have been entrainment of stratospheric air into the anvil. Dickerson et al. also investigated whether simple one-dimensional vertical eddy diffusion models could predict the observed concentrations of trace gases. They found that the short-lived, non-methane hydrocarbon concentrations could not be explained by a slow eddy diffusion model.

In another study during the above experiment, Pickering et al. (1989) measured vertical profiles of CO, O_3 and reactive nitrogen compounds, as well as meteorological variables, on a clear-sky day. Using backward trajectory analyses and photo-chemistry calculations, they concluded that the upper layers of high CO and NO_y concentrations were primarily the result of cumulonimbus venting some 600 km upwind of the central U.S. observation site. Pickering et al. (1990) extended the model calculations described above to a number of cases observed during PRESTORM/PRECP using observations of O_3 precursor gases before and after they were vertically-redistributed by cumulonimbi. They estimated that O_3 production was enhanced by a factor of four due to convective pumping of NO, CO and non-methane hydrocarbons from the boundary layer into the upper troposphere, and NO production by lightning.

Like studies of cumulus clouds, modeling studies of cumulonimbus venting have ranged from two- and three-dimensional cloud models, with bulk microphysics and explicit detailed (bin-type) microphysics, to parameterized cloud models in

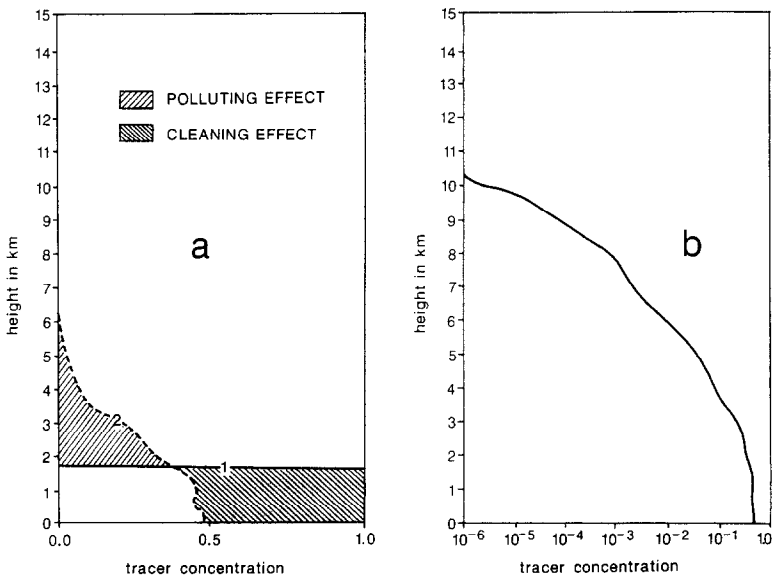

Fig. 7. Horizontal averages of tracer concentrations. Left-hand side: assumed initial vertical profile (curve 1) and calculated profile after 60 minutes of cloud formation (curve 2), right-hand side: the latter profile with logarithmic scaling to emphasize maximum height of transport. The transilient matrix coefficients represent a period of transport starting at $t = 0$ min (15:20 MDT) and ending at $t = 100$ min (17:00 MDT) (from Alheit and Hauf, 1992).

regional and larger-scale meteorological contexts. Alheit and Hauf (1992) added ice-phase microphysics and inert trace gases to Flossman and Pruppacher's (1988) two-dimensional cloud model with explicit bin-resolving microphysics. They applied the model to an ordinary cumulonimbus cloud observed on 19 July 1981 during the Cooperative Convective Precipitation Experiment (CCOPE) (Dye et al., 1986). Following the insertion of a local heat source near the ground, an ordinary cumulonimbus was simulated with a lifecycle (growth, maturity, decay) of approximately one hour, and surface rainfall lasting for 30 minutes. The precipitation efficiency for the cloud as a whole was low, being about 9%. Moreover, only 13% of the total amount of ammonium sulfate aerosol removed by nucleation scavenging was deposited on the ground. By assuming that the two-dimensional simulated cloud was 3 km wide (perpendicular to the model domain), they calculated that the total rain mass was 38,000 tons, and the total sulfur deposition was 450 kg.

Alheit and Hauf (1992) then estimated the change in tracer distribution over the lifetime of the storm by using a transilient matrix C. If X_a and X_b represent the tracer concentrations after and before the convective event, then $X_a = CX_b$. The concentration of the tracer at a specific height is $X_a(i) = \sum_{j=1}^{n} c_{ij} X_b(j)$. The coefficients c_{ij} represent the percentage of air that arrives at the destination level i, from the source level j during the storm lifetime. For an initial tracer distribution that is horizontally homogeneous through a depth of 1500 m (see Fig. 7a), some of the tracer is transported up to the tropopause in less than one hour (see Fig. 7b). For this case, the simulated storm decreased tracer concentrations in the boundary layer by 50% and the air mass transport per unit time was ~30,000 tons per second for an assumed transverse cloud width of 1 km. It increased to ~100,000 tons per second if a transverse cloud width of 3 km was assumed. They noted that this was smaller than mass transports calculated by Heymsfield and Miller (1988) for several other stronger CCOPE storms, including supercells, which ranged from 0.5×10^6 tons per second at 5 km to 1.4×10^6 tons per second

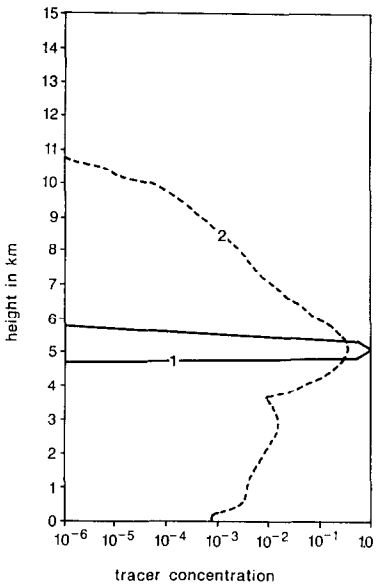

Fig. 9. Application of the transilient matrix (at $t = 100$ min, i.e. after 60 min of cloud activity). Curve 1: initial profile. Curve 2: resulting profile. The transilient matrix coefficients represent the same period of transport as in Fig. 7 (from Alheit and Hauf, 1992).

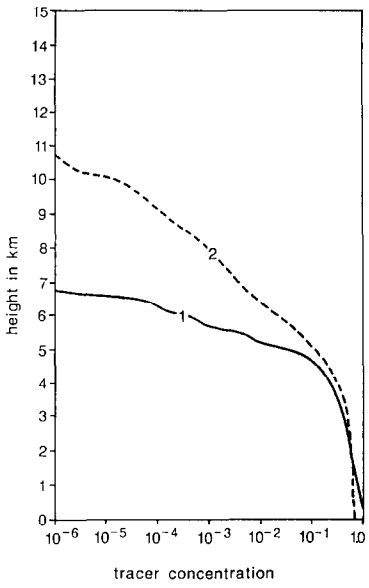

Fig. 8. Application of the transilient matrix (at $t = 100$ min, i.e. after 60 minutes of cloud transport). Curve 1: initial profile. Curve 2: resulting profile. The transilient matrix coefficients represent the same period of transport as in Fig. 7 (from Alheit and Hauf, 1992).

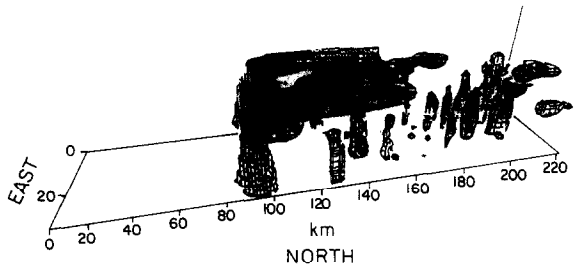

Fig. 10. Three-dimensional view of condensate mixing ratio greater than 0.1 g kg^{-1} at 1300 local time. Shown is the fine grid domain which encompasses the land area; the view is from the north.

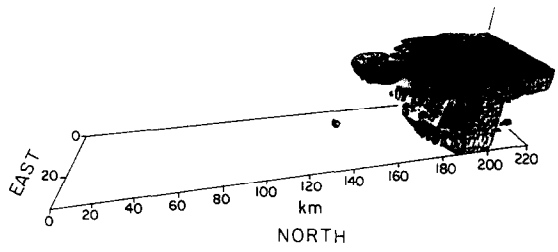

Fig. 11. Three-dimensional view of condensate mixing ratio greater than 0.1 g kg^{-1} at 1800 local time. Shown is the fine grid domain which encompasses the land area; the view is from the north.

at 7 km. This is probably because this is a relatively weak storm.

Alheit and Hauf then modified the initial pollutant profile so that it extended through a deeper layer (Fig. 8). In this case, downdrafts originating in the middle troposphere brought significant amounts of tracer material down to the surface, thus reducing the net upward transport out of the boundary layer. When a thin layer of tracer (Fig. 9) was inserted between 5 and 6 km, the thunderstorm transported material both upwards and downwards. Introduction of the tracer near the tropopause, however, resulted in only very small amounts reaching the surface.

Hertenstein et al. (1992) performed three-dimensional cloud field simulations with RAMS for ordinary south Florida cumulonimbi, over a 400 $\times$ 75 km^2 area with 1.5 km horizontal grid spacing and using bulk mixed-phase microphysics. The simulation was run from early morning to late afternoon, with cumulonimbi forming in response to surface heating and sea-breeze-driven convergence fields. In the early afternoon the lifetimes of the cumulonimbi are about one hour. These more transient storms shown in Fig. 10 exhibit precipitation efficiencies of 33% to 47%. We investigated one hour of the simulation during which three transient cells were active. In this

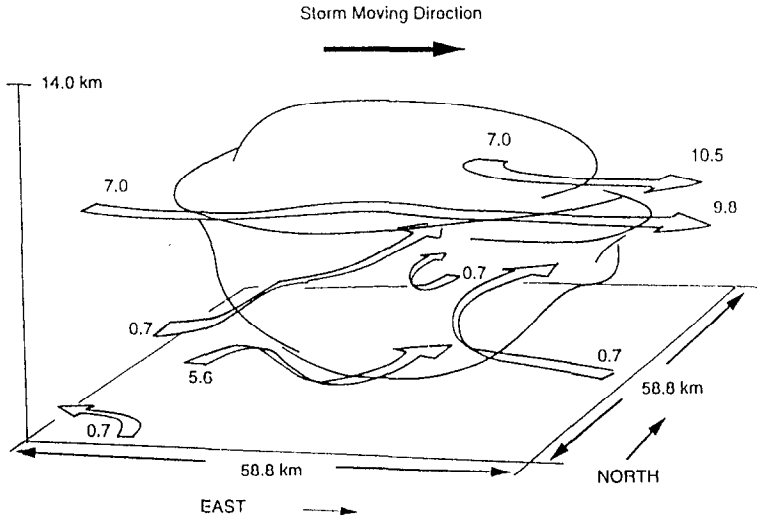

Fig. 12. Diagram of main airflows in the mature stage. The numbers represent the starting heights of these airflows in kilometers (from Wang and Chang, 1993b).

time period, the three cells transported a total of about 3.2×10^{11} kg of boundary layer air. The rate of mass transported by a single transient cell is about 3×10^{7} kg s^{-1}. Later in the afternoon, the sea breeze fronts collide just inland of the west coast and a longer-lived line of steady cumulonimbi is simulated (see Fig. 11). These more efficient rain-producers exhibit precipitation efficiencies of 93%, and together they transport about 6.3×10^{11} kg of boundary layer air in one hour. Each quasi-steady cell exhibits a bulk transport rate of 6×10^{7} kg s^{-1} or a factor of two larger than the more transient cells. Note that this is still one order of magnitude less than the bulk transport rates estimated for supercell storms! This illustrates that within a given class of storm (ordinary cumulonimbi), there is a large variation in the amount of boundary layer air transported.

Wang and Chang (1993a,b,c,d) describe a three-dimensional thunderstorm model that includes a bulk representation of mixed-phase microphysics and seven groups of chemical species involved in air and aqueous-phase chemistry. They simulated a rotating supercell storm observed during the CCOPE on 1 August 1981. During the growth stage of this storm boundary layer air was transported into the middle troposphere (~ 5 km). Once the storm matured, however, air flowed into the storm in four major flow branches, two low-level branches that started at 0.7 km, a mid-level branch (5.6 km) that entered the storm from the south, and upper-level flow branches that entered the storm from the west and northwest (see Fig. 12). They found that the SO_2 which entered the storm at low-levels only affected the lower cloud layer. They also concluded that for surface pollutants with moderate or small solubility, the vertical transport of pollutants by the cumulonimbi exerts the dominant influence on the in-cloud concentrations. They show that the steady, strong flow branches result in supercells having transport characteristics that differ markedly from ordinary, airmass-type cumulonimbi (e.g., supercell flow branches bring air into the cloud from a wide range of altitudes in a systematic way rather than turbulent entrainment of smaller volumes of air).

To estimate the amount of boundary layer mass transported by a single supercell storm, we use a three-dimensional RAMS simulation of the Del City tornadic storm (Ray et al., 1981) using RAMS as described by Grasso (1992). This steady supercell transported 1 to 3×10^{8} kg s^{-1} of boundary layer air; about 1.5 to 4 times greater than the steady Florida thunderstorm. Considering that the typical lifetime of a supercell thunderstorm is roughly three times that of an ordinary cumulonimbus, we see that the supercell transports about 12 times more boundary layer air over its lifetime than a single ordinary cumulonimbus.

Chatfield and Delany (1990) used a one-dimensional, parcel model with photochemistry to examine how the timing of transport of ozone precursor gases by deep convection influences the buildup of tropospheric ozone in tropical regions. They simulated several different scenarios. In one case, pollutants such as NO_x released during biomass burning remain in the ABL and slowly transform into HNO_3 and similar species for a period of 7 days. They are then vented through the troposphere by clouds and removed by lower tropospheric heterogeneous processes. The chemistry of these gases is calculated for another 7 days. In the second scenario, the freshly emitted pollutants are vented by deep convective clouds throughout the troposphere within 4 days of emission. The chemistry of the vented pollutants is then followed for another 10 days. Chatfield and Delaney found the second scenario, which they called the "mix-then-cook" simulation, produced larger amounts of tropospheric column-ozone than the first scenario because the rapidly vented gases were protected from being removed by lower tropospheric chemical reactions and deposition. They suggest that this process could be a contributor to the climatologically high column-ozone inferred by Fishman and Larsen (1987).

Brost et al. (1988) used a three-dimensional regional-scale model to simulate transport of chemical species from North America and Europe to the Atlantic Ocean for the entire month of April 1982. The model horizontal domain was $12{,}000 \times 9000$ km, with horizontal grid spacing of about 190 km. Vertical cloud transport was per-

formed with Walcek and Taylor's (1986) cumulus cloud parameterization. As noted in the previous section, this cloud model was really designed for ordinary cumuli. In this application, however, a wide range of convective conditions were encountered, including those supporting ordinary and possibly severe cumulonimbi. The model explicitly calculated the transport of gases and aerosol, gas-phase chemistry, and anthropogenic emissions of some 24 chemical species. They performed 30 day calculations both with and without clouds. Brost et al. found that clouds increased the total mass of O_3 and HO in the atmosphere by vertically transporting chemical species, which made the atmosphere more oxidizing. Because the photolysis rates increased with height, and because the O_3 produced per NO_x often increases as NO_x decreases, vertical cloud transport increased the total ozone in the domain relative to the cloud-free simulation. Furthermore, they found that clouds decreased O_3 concentrations in the ABL and increased O_3 concentrations in the free atmosphere. This work is just the "tip of the iceberg" in illustrating the complex interactions between clouds and chemical species in the atmosphere.

5. Venting by mesoscale convective systems and tropical cyclones

Mesoscale Convective Systems (MCS's) are deep convective systems which are much larger and longer-lived than ordinary thunderstorms. Typical horizontal dimensions of ordinary thun-

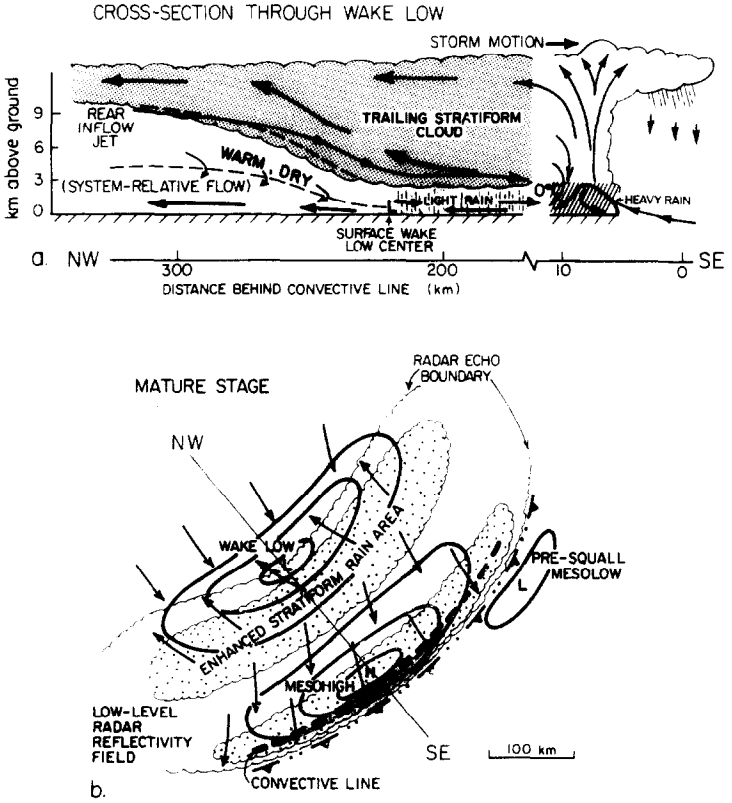

Fig. 13. Schematic cross-section through wake low (a) and surface pressure and wind fields and precipitation distribution during squall line mature stage (b). Dashed line in (a) denotes zero relative wind. Arrows indicate streamlines, not trajectories (adapted from Johnson and Hamilton, 1988).

derstorms are of the order of 10 km, while multicellular thunderstorms may attain dimensions of 25 to 30 km. Typical MCS's, on the other hand, reach a maximum horizontal dimension of about 200 km and in the case of squall lines the long dimension can exceed 1000 km. While ordinary thunderstorms have a lifetime of about an hour, multicellular and supercell thunderstorms may live for 2 to 6 h. MCS's, however, have typical lifetimes of 6 to 12 h. In some cases the remnant circulations and middle-level clouds persist for several days with recurrent intensification to an active MCS (Bosart and Sanders, 1981; Wetzel et al., 1983). The family of MCS's consists of squall lines with a well-defined line of cumulonimbus cells and a trailing and/or leading stratiform anvil, large clusters of thunderstorms that exhibit no distinct mode of cumulonimbus organization but have a large region of stratiform anvil cloud, and mesoscale convective complexes (MCC's) which are large enough to produce a stratiform anvil cloud over 100,000 km^2 in area for at least 6 h (Maddox, 1980).

Thunderstorm cells within MCS's range in intensity from ordinary cumulonimbi to severe supercells. A severe, pre-frontal squall line, for example, may consist of a line of cells 1200 km long with mostly supercells. The cloud-venting or transporting properties of MCS's are, therefore, like those of individual thunderstorms except there are more of them and they collectively last longer. In addition, MCS's consist of slantwise mesoscale ascending and descending branches of air. The convective updrafts and slantwise slowly ascending branches can have greatly different cloud-venting properties because the time scales for ascent in an aqueous environment differ. This affects both chemical reactions and scavenging processes. Fig. 13 illustrates a mid-latitude squall line with a leading convective line and a trailing stratiform cloud with an ascending front-to-rear branch and a descending rear-to-front branch. In the stratiform anvil region of some MCS's the slantwise flow branches can become quite complex. Fig. 14 illustrates the flow branches in an MCC which contains an ascending front-to-rear branch, middle-level, moist, descending cool airstream and two middle- or upper-level dry descending branches.

Clouds and precipitation in the stratiform anvil cloud are the product of detrainment of hydrometeors from the active cumulonimbus cells and in

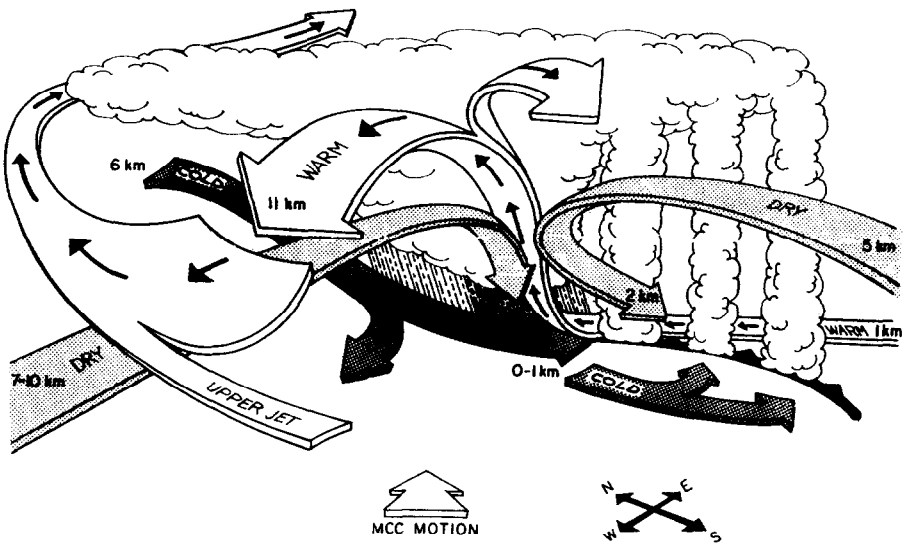

Fig. 14. Perspective drawing of an idealized, weakly rotating mesoscale convective complex as viewed from the rear. The apex region is located where the heavier rain is drawn. The cumulonimbus towers at right form on the mesoscale cold front. The mesoscale warm front and the forward part of the stratiform region are not shown in this view (from Fortune, 1989).

situ condensate production by air ascending at speeds of 0.1 to 1.0 m s^{-1}. These slantwise branches can slowly transport trace gases and pollutants vertically through much of the troposphere, while providing an environment for sustained aqueous chemical reactions. Moreover, they are also sites for sustained production of trace gases by lightning. Goodman and MacGorman (1986) showed that MCC's produce maximum cloud-to-ground lightning strikes of 54 min^{-1} averaged over 1 h and in excess of 17 min^{-1} for nine consecutive hours! They concluded that the passage of a single MCC over a given location can produce 25% of the mean annual strike density at that site.

MCS's are generally believed to be efficient rain producers. Precipitation efficiency estimates for mature mid-latitude MCC's have exceeded 100% because a considerable part of the rain that falls during the mature stage is a result of water substance that has been injected into the middle and upper troposphere during its growth stage. Precipitation efficiencies for MCS's averaged over the system's lifetime probably exceed 70% but quantitative estimates have yet to be made. Nonetheless, it appears that MCS's are very efficient scavengers of pollutants from the atmosphere.

Tropical cyclones are close cousins to MCS's. Like MCS's they derive most of their energy from the latent heat released in rising convective towers and slantwise ascending branches of air. Large MCS's like MCC's develop an inherent inertial stability in which they often exhibit a middle-level cyclonic circulation and upper-level anticyclonic circulation (Cotton and Anthes, 1989). This inertial stability is an important factor in the maintenance of the bigger MCS's for lifetimes of 12 h or more. In that sense a mature tropical cyclone represents the most inertially stable member of the family of MCS's allowing it to survive as a mature named tropical storm for 10 days or more.

Like MCS's, tropical cyclones consist of deep convective cells and slantwise ascending and descending flow branches. Fig. 15 illustrates schematically the locations of the deep convective

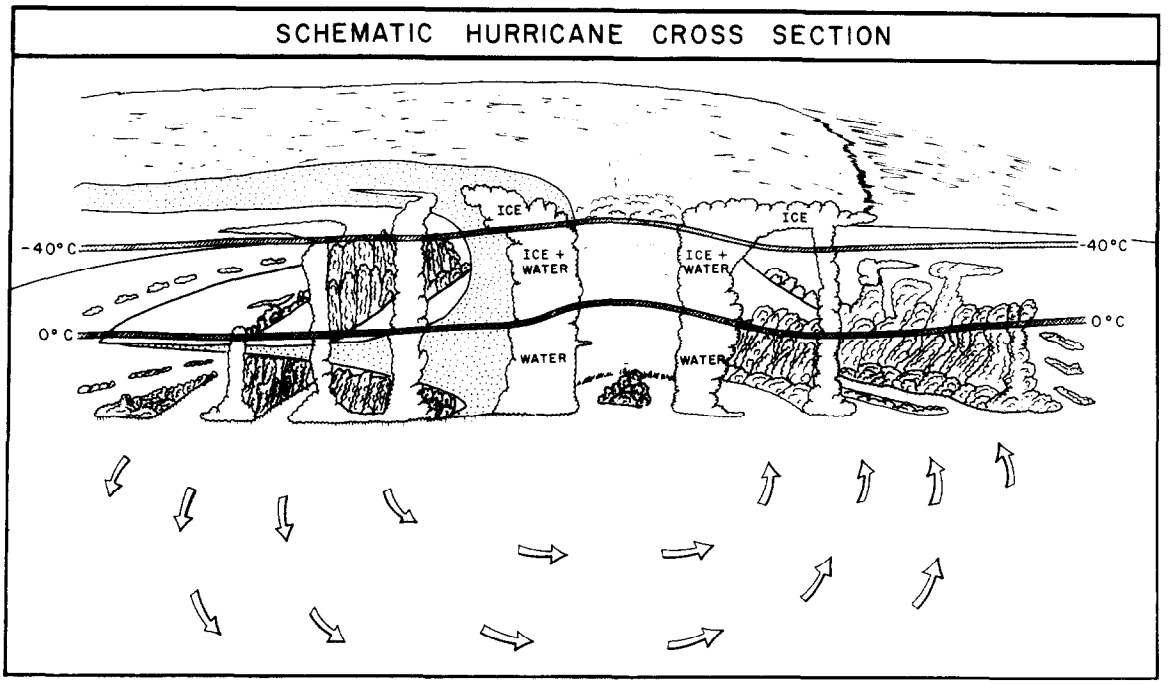

Fig. 15. Schematic diagram of hurricane showing low-level circulation and cloud types. The highest clouds, composed of cirrus and cirrostratus, occur at the tropopause which is about 16 km (From Stormfury, 1970).

cells. Generally the most intense, steady cumulonimbi reside in the eyewall region. Outward from the storm core, towering cumuli and more transient cumulonimbi reside in the inner rainbands. Further out in the outer rainbands towering cumuli and occasional cumulonimbi are encountered. Most of the deep convective vertical transport is concentrated within about 200 km of the storm center. Like MCS's, tropical cyclones are efficient rain-producers and therefore can be expected to be efficient scavengers of pollutants. At this time there do not appear to have been any systematic studies of the role of tropical cyclones in venting of trace gases or pollutants.

To the authors' knowledge, there has been only one observational paper that focuses on the cloud venting properties of MCS's. Lyons et al. (1986) analyzed ozone and visibility data as well as conventional meteorological data for a 31-h period on 1–2 August 1980. During this period three MCS's formed and propagated through the southeastern United States. One system, which formed over southeastern Missouri, met Maddox's (1980) criteria for an MCC, while a second over Maryland and Delaware was a smaller convective cluster, and the third was a squall line that formed in North Carolina. These systems depleted largely surface-generated afternoon ozone amounts from 100–1200 ppb to 20–40 ppb. Moreover, visibility increased from 4–13 km to 27–80 km, in a matter of a few minutes at many locations. Lyons et al, estimated that these systems removed 3×10^7 kg of sulfate from the ABL. They estimated that two-thirds of the sulfate removal from the ABL was by thunderstorm venting to altitudes as high as the tropopause, with the vented air being

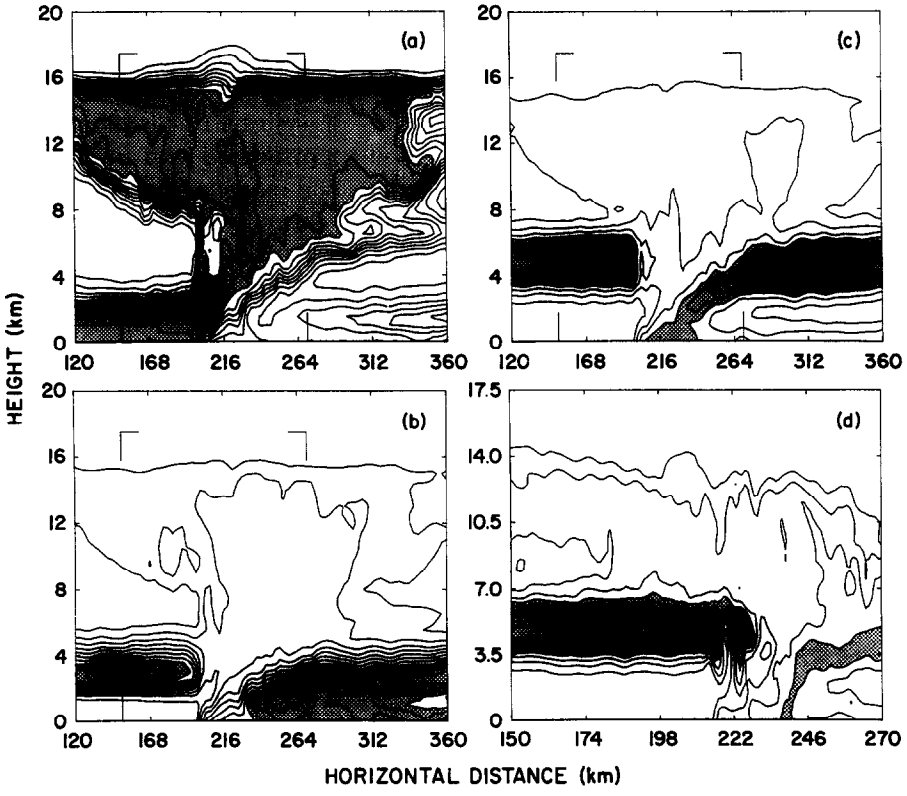

Fig. 16. Tracer fields after 6 h of simulation (a) tracer 1 in simulation 23Z in domain 2, (b) tracer 2 in simulation 23Z in domain 2, (c) tracer 3 in simulation 23Z in domain 2 and (d) tracer 3 in simulation 23U in domain 3. The dotted regions show where the tracer is in excess of 50% concentration in (a) and (b), 25% in (c) and (d). The isoline interval is 6.25% and the bracketed regions in (a), (b) and (c) correspond to domain 3 (from Lafore and Moncrieff, 1989).

replaced with cleaner mid-tropospheric air brought down by convective downdrafts and slowly descending mesoscale air streams.

Modeling studies of venting by squall lines have been mainly two-dimensional. Because squall lines frequently exhibit considerable symmetry about the vertical plane perpendicular to the squall line gust front, they offer the opportunity to reduce computational costs by using a two-dimensional model. Lafore and Moncrieff (1989) analyzed the transport of passive tracers in their simulation of West African squall lines. They introduced passive tracers with concentrations of unity in three layers. The first tracer was introduced in the 0–2 km layer, the second was introduced from 2–4 km, while the third was in the 4–6 km layer. Fig. 16 illustrates that the low-level tracer (tracer 1) is efficiently transported into the upper troposphere. The shaded area in Fig. 16a shows that there is a large region in the upper troposphere where the concentrations are in excess of 50% of the values in the ABL. Tracers 2 and 3, initially released between 2 and 6 km, are mostly transported downwards into the low-level cold pool. Only 10–15% of the initial tracer reaches upper levels. The above boundary layer tracers mostly enter the storm from the rear of the system, although with a stronger jet at mid-levels tracer 3 enters the storm mainly from ahead of the line.

Like Lafore and Moncrieff, Nicholls and Weissbluth (1988) performed two-dimensional simulations of tropical squall lines and released passive tracers into the simulated flow fields. They also performed quasi-three-dimensional simulations of the same storm in which RAMS was set up with a 30-km wide channel with cyclic boundary conditions that was oriented perpendicular to the squall line. Fig. 17 illustrates the depiction of the passive tracer released ahead of the squall line at the 0.0–2.0 km layer (Fig. 17a) and the 2.0–4.5 km layer (Fig. 17b). The results show that as much as 40% of the low-level air is transported as high as 12 km, while only small amounts of the air in the 2.0–4.5 km layer are transported aloft.

Garstang et al. (1988) used a two-dimensional mesoscale/cloud model to help in the interpretation of chemical observations taken by aircraft during the NASA Amazon Boundary Layer Experiment (ABLE 2A). Two cloud systems were studied, one being quite linear and amenable to two-dimensional simulations, the other being more of a cluster of cumulonimbi and thus not as well approximated with a two-dimensional model. The cloud model was used to simulate the transport of chemical species which were sampled with the aircraft. For example, they inferred that enhanced concentrations of CO near the surface were due to downdraft transport of pollutants

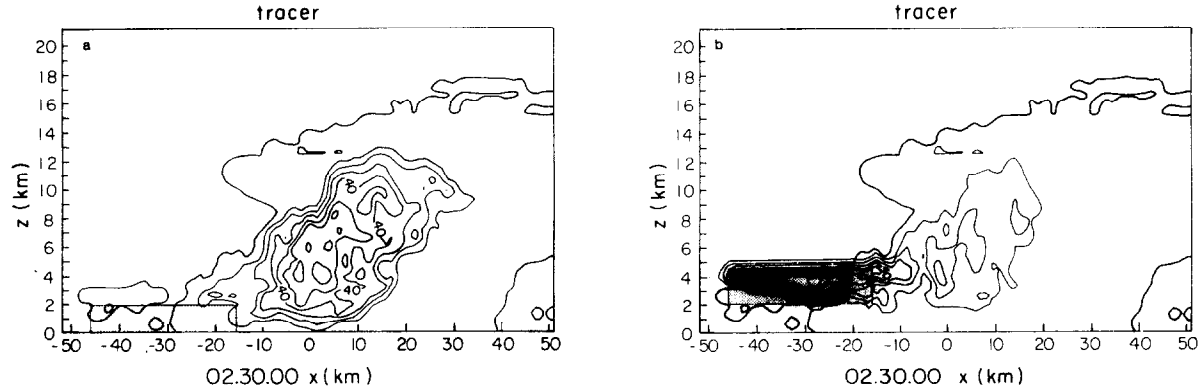

Fig. 17. Vertical cross-section showing tracers introduced ahead of a three-dimensional simulation of a squall line. (a) 0.0–2.0 km, and (b) 2.0–4.5 km. Shading shows the initial position of the tracer with a concentration of 1 g kg^{-1}, introduced at 1.5 h. The contours indicate the position at 2.5 h. The contour interval is 0.1 g kg^{-1} and the label scale is 100 (from Nicholls and Weissbluth, 1988).

residing in a well-defined haze layer between 1.5 and 2.5 km.

In another study Scala et al. (1990) used the above two-dimensional model and a one-dimensional photochemistry model to help interpret surface and upper-air chemistry observations for a squall line event during NASA ABLE. Individual Lagrangian particle tracers were released to identify the major flow branches of the simulated squall line (see Fig. 18). Clearly evident is a nearly vertical displacement of boundary layer air in convective updrafts to where cooling by melting of hydrometeors and entrainment of dry environmental air by a mid-level jet were inferred to produce strong detrainment. Further ascent occurs in more slantwise front-to-rear mesoscale flow branches. Downdraft branches consist of a shallow overturning downdraft behind the updraft cores. This appears to resemble the "up-down" downdraft branches modeled and observed by Knupp (1985) in mid-latitude thunderstorms. Mesoscale slow descent originating near the melting level produced a rotor circulation at the 4.5 km level. Scala et al. (1990) also released 6 levels of tracers into the model domain (see Fig. 19) similar to Lafore and Moncrieff (1989). Forty percent of the initial concentration of tracer 2 reaches the 3.5 km level. Likewise, downdraft

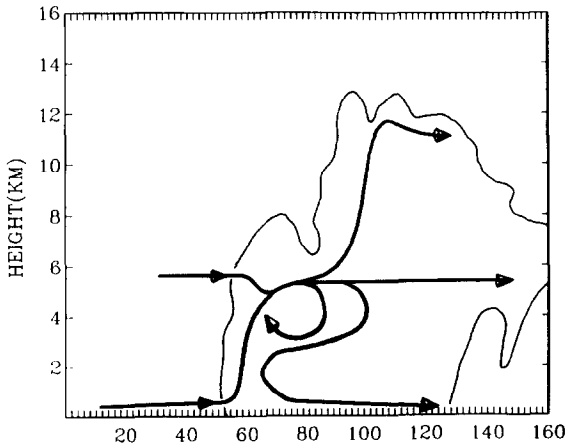

Fig. 18. Composite schematic of the predominant transport pathways for the May 6, 1987, model squall convection based on forward and backward trajectory analyses. The model cloud outline at 300-min simulation is included. The horizontal dimension is 160 km (from Scala et al., 1990).

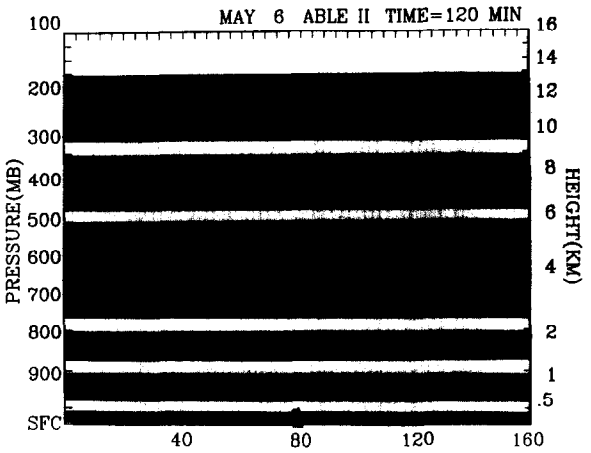

Fig. 19. The initial composite distribution of six inert tracer layers introduced into the simulation at 120 min. The vertical dimensions of each are tracer 1, 0.0–0.10 km; tracer 2, 0.31–0.81 km; tracer 3, 1.10–1.73 km; tracer 4, 2.09–5.21 km; tracer 5, 5.74–8.21 km; and tracer 6, 8.78–12.39 km (from Scala et al., 1990).

transport of tracer 2 results in 40% of its initial concentration reaching the surface 40 km behind the updraft cores. About 40% of tracer 3 is transported upward by the convective cores, while about 20% is caught up in the "up-down" downdraft branch and is transported to within 200 m of the surface. Most of the air in the anvil region is composed of tracers 5 and 6 with concentrations 40% of their initial values. Calculations with the one-dimensional photochemical model suggest that ozone chemical destruction in the boundary layer cannot account for the observed changes, so that convective transports have a dominant effect on low-level ozone concentrations.

In yet another NASA ABLE 2A case study, Pickering et al. (1991) used the same cloud model and a photochemistry model to calculate the effects of cloud venting on tropospheric chemistry. This squall line occurred during the dry season and was much more vigorous in transporting boundary layer air aloft than the wet season storm described by Scala et al. As in Scala et al. the layered tracer scheme was used to transport passive scalars in the two-dimensional simulated flow fields. In this case, however, initial soundings of CO, O_3 and NO_x were fed into the tracer

fields and then the actual concentrations of those fields were calculated based on the modeled transport. The results showed that the polluted concentrations of CO in the boundary layer were transported into the upper troposphere, with increases of more than 60 ppb between 2.5 and 6 km, and 20 ppb up to 12 km. Likewise, the lower concentrations of O_3 in the boundary layer compared to the upper troposphere, produced decreases in O_3 of 30 ppb at 12 km level and decreases of more than 10 ppb in a large region above 5 km. Downward transport of the low-concentration CO into the polluted boundary layer by downdrafts within the squall line reduced CO concentrations by 80 ppb.

Pickering et al. applied their one-dimensional photochemistry model to these vertically-redistributed profiles of trace gases. The chemical model was run for local noon in, and a few kilometers ahead, of the squall line. Pickering et al. estimated in-cloud photolysis rates and wet removal rates, and calculated the diurnally-averaged ozone production rate for air that has been processed by the storm and for undisturbed air ahead of the storm. They found that at noon, when the storm was mature, the instantaneous ozone production potential in the storm was 50–60% less than for no-cloud conditions, due to decreased photolysis and cloud scavenging of radicals. They also found that during the 24 h-period following convection, the total ozone production was little changed from pre-storm conditions. A change from net ozone destruction to net production occurred, however, in the middle to upper troposphere as a result of storm venting.

We have applied a Lagrangian particle dispersion model to a three-dimensional RAMS simulation of the MCS probed by research aircraft on 2–3 February 1987 during the ninth flight mission of the Darwin, Australia-based Equatorial Mesoscale Experiment (EMEX9). The model, initialized with the a horizontally variable (1.25° latitude/longitude spacing) data set, was run with three interactive grids, with the finest having 1.5-km spacing. Fig. 20 shows the 0.5 g kg^{-1} surface of condensate mixing ratio. It shows the extent of the convective towers and the stratiform-anvil cloud. The Lagrangian particle dispersion model (LPDM) was used to illustrate system-relative particle trajectories for the simulation (not shown). In a system-relative sense, particles released at 1 km at 1430 UTC move from front to rear over 90 min. Two ascending flow branches are evident — one on the west-central part of the grid in which particles travel slantwise front-to-rear from low levels to 6 or 7 km, and another in the south-central part in which rising parcels reverse from in a front-to-rear to rear-to-front once

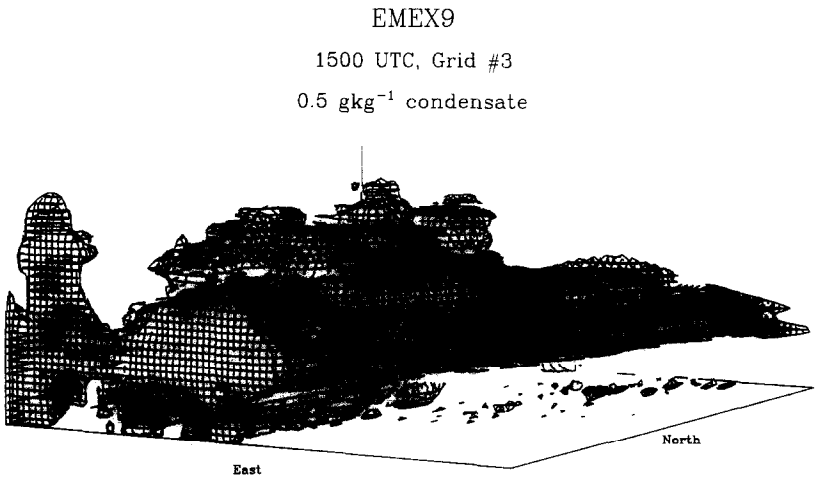

Fig. 20. The 0.5 g kg^{-1} condensate surface on Grid #3 of the RAMS simulation of EMEX9. Perspective is from the northeast. The east–west, north–south and vertical scales are 147 km, 123 km and 20 km, respectively.

they get to about 4 km. Particles released at 7 km conspicuously trace out the top-half of the front-to-rear branch. Particles not caught up in this branch are advected eastward by the prevailing monsoon westerlies. Backward trajectories from the middle of the ascending front-to-rear branch suggest that most of the air feeding that branch originates in the 3–5 km layer, not the ABL. Ordinary cumuli may feed this layer with boundary layer air outside of the active MCS, but it appears little boundary layer air is directly ingested into the front-to-rear circulation by the active MCS.

We find that 32% of the particles are displaced from the boundary layer, primarily by deep convective updrafts. Assuming that this also means that 32% of the boundary layer air is displaced, we infer that approximately 6.72×10^{12} kg of air are removed from the fine grid's boundary layer between 1430 and 1600 UTC, or 1.24×10^{9} kg s^{-1}. As little of 5% of the vented boundary layer air, however, is transported above 5 km. As expected, precipitation efficiencies for the tropical MCS are high, ranging from 30% during early convective growth to 65–76% during maturity.

A simulation of an intense mid-latitude squall line, observed on 10–11 June 1985 during PRESTORM (Cunning, 1986), was performed with RAMS using four nested grids with horizontal meshes ranging from 80 km to 2.22 km. The fine grid was located to explicitly resolve both the convective line and the stratiform precipitation regions during the mature stage of the storm. Fig. 21 is a three-dimensional perspective of the 0.1 g/kg surface of liquid water content, showing the characteristic core of high liquid water content in the convective region and the deep, extensive, trailing stratiform-anvil cloud. This system exhibited an intense leading line of convection, a slantwise, mesoscale front-to-rear ascending branch, and a trailing descending rear-to-front flow branch. As in the EMEX-9 tropical system, most of the air feeding the ascending front-to-rear branch originated in the 3 to 5 km layer, not the ABL. Calculated precipitation efficiencies increase from 38% early in the convective growth stage to over 113% during the mature stage, and then decrease to 40% as the convective line weakens and stratiform precipitation begins to prevail. The calculated boundary air mass transport for this mature squall line 5.5×10^{9} kg s^{-1}. During the analysis time, 75% of the vented ABL air is transported upward by cumulonimbi above 12 km. These intense convective cells transport a great deal more boundary layer air into the upper troposphere than the weaker cells simulated in the EMEX9 MCS. Little of the boundary layer air, however, was transported through the tropopause at 14 km.

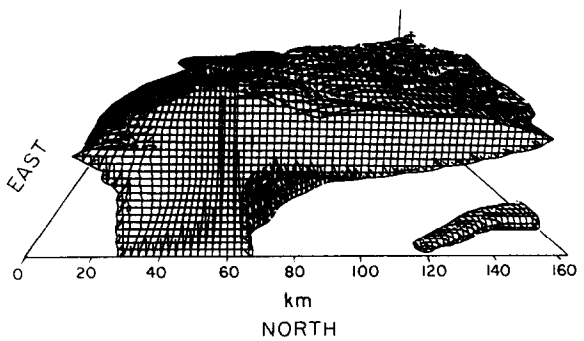

Fig. 21. Three-dimensional view of condensate (greater than 0.1 g kg^{-1}) for the 2.22 km grid at 0500 UTC. The view is from the north.

A pioneering observational study by Riehl and Malkus (1961) addressed boundary layer venting in a tropical storm. Based on aircraft and ship observations, they performed numerous mass flux and budget calculations for the core region (out to 148–185 km) for a period when the storm was just short of hurricane strength, and again two days later when it was a strong hurricane ($\sim$ 60 m s^{-1} maximum winds). On both days, they found good agreement between the mass inflow in the 1000–900 mb subcloud layer (which tripled from about 2×10^{9} kg s^{-1} to 6×10^{9} kg s^{-1} over the two days) and vertical mass flux by "hot towers" to the upper troposphere.

We have made similar estimates of boundary layer venting by tropical cyclones based on three-dimensional convectively-explicit, nested grid simulations with RAMS. A fine-grid increment of 5 km was used on a 400×400 km^2 domain. The environment was based on a composite West Indies sounding for the "hurricane

season" (Jordan, 1958). This mean sounding was moistened to more accurately represent a hurricane environment (Gray et al., 1975). The simulation was initialized with a deep vortex in gradient wind balance (maximum winds of 20 m s^{-1}). Low-level convergence caused by surface friction led to rapid development of deep convection. Fig. 22 shows a horizontal cross-section of wind vectors and total condensate at $z = 5.3$ km and $t = 12$ h. A cyclonic vortex is evident with tangential wind speeds of ~ 30 m s^{-1} at this level. A relatively cloud-free eye of radius 30 km is apparent at the center of the vortex. At this stage there are two intense convective cells. In the fine grid domain the mass flux due to updrafts (> 10 cm s^{-1}) at the level $z = 911$ m is 5.5×10^9 kg s^{-1}. Over the period of a day this is equivalent to venting, through this level, a layer of air 911 m deep and having an area 4.6×10^5 km^2. Considering the slightly larger area of computation and the relative strength of the simulated tropical cyclone, this figure accords well with the mass fluxes inferred by Riehl and Malkus (1961). The mass flux due to downdrafts (< 10 cm s^{-1}) through the 911 m level is 3.3×10^9 kg s^{-1} indicating that small-scale downdrafts are responsible for injecting a considerable quantity of air into the boundary layer. The precipitation efficiency based on the vapor flux at the level $z = 1557$ m was approximately 90%.

6. Cloud venting by extratropical cyclones

Extratropical cyclones are the most prolific cloud-producing systems in middle and high latitudes. Their principal driving force is the poleward temperature decrease, usually concentrated in rather narrow baroclinic zones or fronts. These baroclinic zones become unstable with respect to wave-like perturbations, resulting in the development of cyclones there. The wavelength of maximum instability depends on the static stability and horizontal temperature gradient (Staley and Gall, 1977) and is on average about 3000 km. As a cyclone develops, cold air is carried equator-

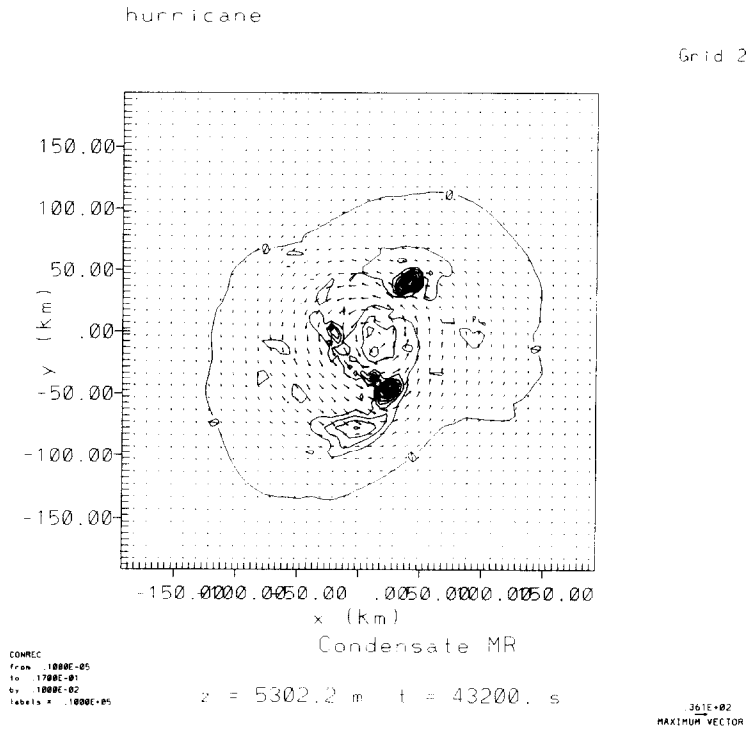

Fig. 22. Horizontal cross-section of hurricane simulation at $z = 5.3$ km. Wind vectors shown with a maximum wind speed of 36 m s^{-1} and total condensate contoured at intervals of 1 g kg^{-1}.

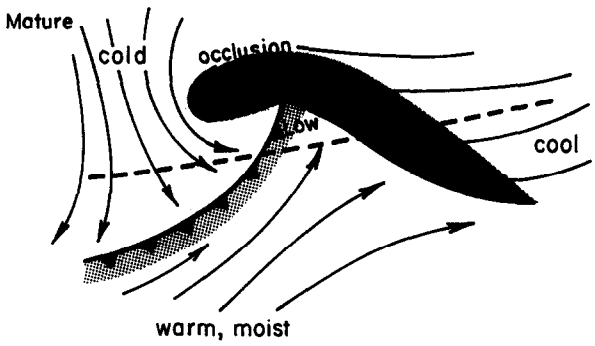

Fig. 23. Schematic of a mature extratropical cyclone according to the Norwegian model. Shaded areas are regions of precipitation.

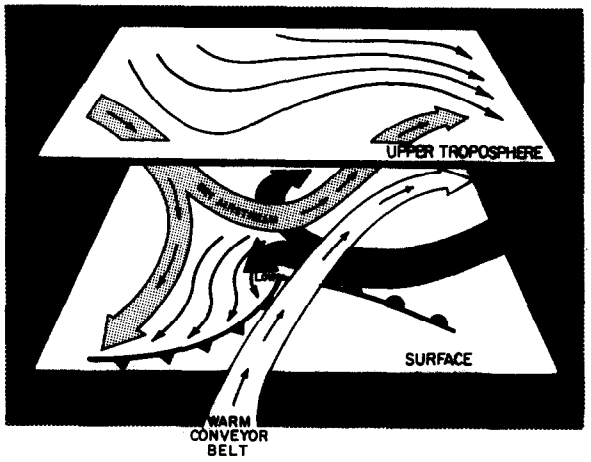

Fig. 25. Schematic of three major airstreams associated with a strengthening extratropical cyclone: warm conveyor belt; cold conveyor belt; dry airstream of stratospheric air intruding into the troposphere (adapted from Kocin and Uccellini, pers. commun.).

ward to the rear of the system and warm air is carried poleward ahead of it. This is illustrated schematically in the classic Norwegian model of a mature extra-tropical cyclone in the Northern Hemisphere (Fig. 23).

A west–east cross section through the mature storm illustrates the types of clouds one can encounter (see Fig. 24). In the warm frontal region the prevailing cloud types are mostly stratiform in character, being driven by slowly ascending airstreams. Along the cold front where stronger ascent occurs and the air in the warm sector generally contains large amounts of CAPE, deep convective clouds are common. Behind the cold frontal boundary, shallow cumulus clouds are generally found. The air feeding these clouds can come from long distances as they slowly ascend or descend in the major slantwise flow branches of the extra-tropical cyclone. Fig. 25 illustrates the warm conveyor belt, the cool conveyor belt, and the dry airstream identified by Carlson (1980) as the major flow branches of the storm.

One can see that the venting characteristics of clouds within extra-tropical cyclones vary considerably with their location within the storm. Moreover, the properties of the low-level airmass feeding those clouds vary with the trajectory of the airstream, as well as with the sources and sinks of gases and aerosol along the major flow branches. There is also considerable variability in the characteristics of extra-tropical cyclones. Some mid-winter cyclones may have little convection and be dominated by stratiform precipitation. Other cyclones, such as rapidly deepening coastal cyclones

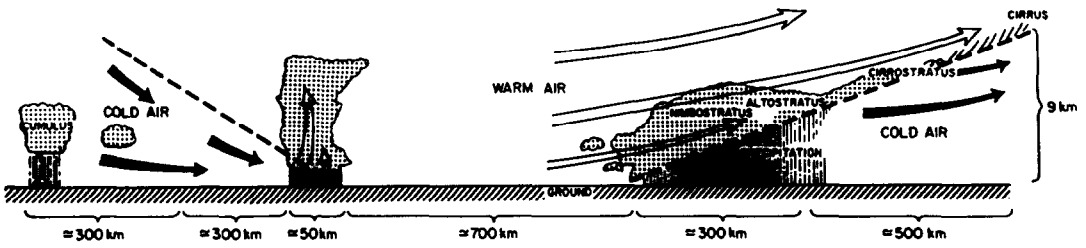

Fig. 24. Schematic vertical cross section through an extratropical cyclone along the dashed line in Fig. 23, showing typical cloud types and precipitation (adapted from Houze and Hobbs, 1982).

(e.g., Sanders and Gyakum, 1980) are strongly affected by deep convection.

Most of the research on cloud venting by extra-tropical cyclones has focused on the use of numerical models and, furthermore, has concentrated on specific sub-features of the cyclone rather than the effects of the storm as a whole on vertical redistribution of pollutants. Banic et al. (1986), for example, examined the vertical transport of pollutants by weak cold fronts using instrumented aircraft observations of cloud physics and chemistry, together with the Hoskins and Bretherton (1972) analytical model of fronts. The observations revealed an elevated maximum in aerosol concentrations in the frontal zone. In the modeling study, Banic et al. assumed that the initial aerosol concentrations varied linearly across the frontal zone with highest concentrations ahead of the front, and that the aerosol concentrations decayed exponentially with height in the pre-frontal and post-frontal air masses. Like the observations, the Hoskins–Bretherton model predicted an elevated maximum of aerosol concentrations above the frontal surface as shown in Fig. 26.

Hybrid observational and modeling studies of cloud transports of pollutants by warm and cold fronts has been accomplished by feeding radar and sounding data into diagnostic cloud and atmospheric chemistry models. In this approach (see Hegg et al., 1984,1986; Rutledge et al., 1986; Barth et al., 1992), dual Doppler radar observations are used to identify the vertical and horizontal distribution of winds associated with specific fronts. Using the observationally-derived air motions and a local sounding of temperature and relative humidity, the Rutledge and Hobbs (1983) two-dimensional kinematic cloud model is then run to calculate the steady-state microphysical structure of the frontal feature.

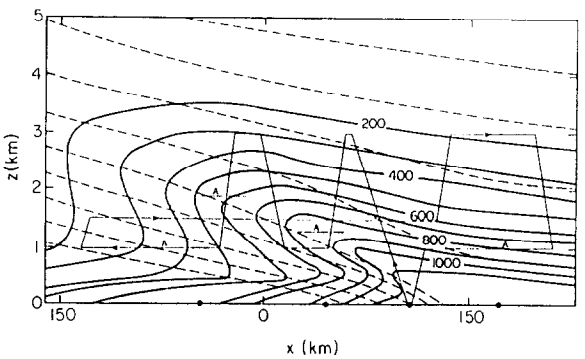

Fig. 26. Model results for initial aerosol distribution II. The dashed lines are intervals of θ where $\Delta\theta = 2.6$ K and the heavy solid lines are the aerosol concentrations. The light solid line shows an idealized flight plan for sampling the chemical constituents of the air masses and frontal zone. Appropriate ground sampling sites are indicated by • (from Banic et al., 1986, reprinted by permission of Kluwer Academic Publishers).

These model-calculated cloud fields are then used to drive an aqueous and gaseous chemistry model describing the sulfur cycle with an emphasis on total sulfate deposition. This approach is strictly valid only if the air motions are steady during the simulation period. Verlinde and Cotton (1990) have shown that the application of the technique to unsteady wind fields, such as in cumulus clouds, can lead to significant errors in the derived cloud microphysical fields. In non-steady cases, the time history of the cloud is important, and more complex algorithms such as those developed by Verlinde and Cotton (1993) are required. Nonetheless, application of the kinematic cloud/chemistry model to steady warm-frontal rainbands (Hegg et al., 1984), to narrow cold-frontal rainbands (Hegg et al., 1986; Rutledge et al., 1986) and to narrow and wide frontal rainbands (Barth et al., 1992) has revealed considerable insight into the complex processes affecting surface deposition of chemical species.

A variety of two-dimensional models have been used to examine the transport properties, cloud physics and chemistry associated with fronts. These have ranged from simple semi-geostrophic models of frontal circulations (Kavassalis et al., 1986) to schematic models of warm-frontal rain (Cho et al., 1986), to two-dimensional numerical prediction models of frontal systems (Chaumerliac et al., 1992). Chaumerliac et al., for example, concluded that efficient vertical transport of pollutants occurs only when clouds are present.

At this point there have been only a few applications of fully three-dimensional numerical prediction models to the simulation of cloud trans-

ports in extra-tropical cyclones. Walcek et al. (1990) applied the regional acid deposition model (RADM) described by Chang et al. (1987) to a three-day spring-time period over the northeast U.S. in which a extra-tropical cyclone passed through the region. Cloud transport is simulated within RADM with the one-dimensional cloud model developed by Walcek and Taylor (1986) and described in Section 3. The simulation showed that ozone formation rates are enhanced by ~50% when cloud transport of surface-emitted nitrogen oxides and organic compounds into the upper troposphere occurs. Moreover, because the genesis of extra-tropical cyclones occurs in association with upper tropospheric jets, the vented NO_x is rapidly advected horizontally over large areas contributing to enhanced global production of tropospheric ozone.

7. Global estimates of annual boundary layer mass flux and precipitation by cloud systems

In preceding sections we reviewed the literature on venting of boundary layer air by various cloud systems. In order to help global modelers in prioritizing where to put their efforts in developing and refining cloud transport parameterization schemes, it might be useful to estimate the global average contribution of each deep cloud system to venting of boundary layer air. To do so, however, requires many assumptions, so the results should be interpreted largely as order-of-magnitude estimates only. Our approach is to estimate the total cloud venting contributions by various populations of cloud systems and to combine quantitative aspects of representative systems (obtained either observationally or from modelling) with their climatologies.

7.1. Annual precipitation

Global annual precipitation

We begin with a globally averaged annual precipitation rate of 1000 mm yr^{-1} (Palmen and Newton, 1969). When multiplied by the area of Earth (5.10×10^8 km^2), this gives a total annual precipitation mass of 5.10×10^{17} kg. We assume that 5% of this total is due to non-venting types of systems, such as orographic and mid-level-based precipitation, both in the tropics (30°S to 30°N) and midlatitudes. The remaining 95%, or 4.85×10^{17} kg, is the figure used as a cumulative total of annual precipitation mass produced by all populations of cloud venting systems (Table 1).

Tropical annual precipitation

For an annual mean precipitation over the tropical belt from 30S to 30N, we use 3.47 mm day^{-1}, which is the average of three climatological estimates provided in Janowiak (1992). With half of Earth's surface area, this tropical precipitation amounts to 3.23×10^{17} kg yr^{-1}, or 63% of the global total precipitation.

Tropical convective system precipitation

Machado and Rossow (1993) provide size distributions of cold-topped convective cloud systems, as defined by an infrared temperature of −28° C, for four geosynchronous satellite regions, each covering an area from about 30S to 30N and about 80 degrees of longitude. The results are based on 1200 Local Standard Time (LST) observations daily during two Januarys and Februarys and two Julys and Augusts. These four distributions, in terms of average number per day in each size category, were very similar, and collectively cover most of the tropical belt. We combined these distributions and extrapolated for another 40 degrees longitude to estimate complete tropical coverage, and then multiplied the distribution by 365 days to estimate an annual frequency distribution. This assumes (fairly reasonably) that the Machado and Rossow size distribution is representative of all months.

When the resultant annual size distribution is plotted as log $N(A)$ vs. log A or as log $N(R)$ vs. log R [where $N(A)$ or $N(R)$ are number in a size class of area A or radius R, respectively], it is very nearly a straight line, which can be approximated by a power law relation of the form $N(R) = N(0)R^{-\alpha}$ where $N(0)$ and α are constants. The relation which best fits the Machado and Rossow distribution is shown in Fig. 27 as the bold dashed line, with the asterisks denoting their size classes.

Note that this distribution, in number of MCS's per year in each size class, is not based on maximum cloud sizes during their lifetime (as with MCC surveys discussed later), but represents the instantaneous convective system size distribution as seen in 365 daily satellite observations at 1200 LST.

We next assume that the annual distribution based on 1200 LST observations is representative of all hours. This may not be a very good assumption, however, since Machado et al. (1993) show for tropical Africa and eastern Atlantic that there is a diurnal dependence on total cloud cover (particularly over land) and on the size distribution. In the Area–Time Integral (ATI; Doneaud et al., 1984) [1] precipitation estimation technique

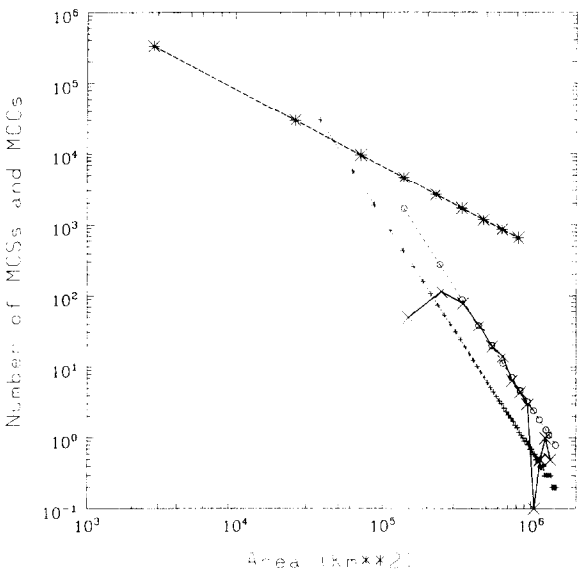

Fig. 27. Frequency distributions (in number/year) of various convective system populations as a function of system size. Bold solid curve is observed MCC distribution based on Laing and Fritsch (1993), with large crosses denoting mid-points of size classes in increments of 100,000 km^2. Thin dashed curve with the same 100,000 km^2 size classes marked with circles is power-law relation based on the Laing/Fritsch curve. Thin short-dashed curve is the same, except 100,000 km^2 size classes are subdivided into 25,000 km^2 sizes (small plusses) and curve is extended to smaller size classes. Bold dashed curve is power-law relation based on tropical observations by Machado and Rossow (1993), where large asterisks denote mid-point equivalent radius (converted to area) of their size classes.

used below, however, the distribution of total cloud cover over the size classes does not affect the total estimated precipitation and we adjust for the deviations of 1200 LST cloud cover over both land and oceans from their average coverages.

Based on the above assumptions, a total annual ATI can be calculated for each size class, with the cumulative total representing a fairly reliable observationally derived annual cloud cover by tropical convective systems. Then, using a simple precipitation estimation scheme, $V =$ (mean P) $\times$ ATI, where P is the precipitation rate, the total precipitation volume due to these convective systems can be estimated. Janowiak (1992) cites a mean P of 3 mm h^{-1} for clouds defined by a a threshold of $-38°$ C. Machado and Rossow's (1993) distributions are based on a threshold of $-28°$ C, which according to more geographically limited statistics in Machado et al. (1993), identifies clouds about 1.5 times larger than the $-38°$ C threshold, suggesting that P needs to be scaled accordingly to about 2 mm h^{-1}. However, to account for the 1200 LST deviations from the average coverage seen in Machado et al. (1993), this rate was adjusted upward to 2.14 mm h^{-1}, based on large upward and small downward corrections over land and ocean, respectively, weighted by the fractions of land and ocean in the tropics. Thus, the V–ATI relation yields an estimated annual tropical precipitation mass of 3.00×10^{17} kg. This value is 93% of the climatological tropical precipitation. The remaining 7% is assumed to be 5% due to non-venting related precipitation, as stated earlier, and 2% due to non-convective precipitation associated with the few extratropical cyclones that occur equatorward of 30° (more later).

Global convective system precipitation extrapolated from tropics

There is little information on the global size distribution of convective systems similar to

[1] ATI is the time integral of cloud area as defined by a particular threshold, in units of area × time.

Table 1
Annual contributions by characteristic cloud systems

System type	Size (km^2)	Duration	Total precipitation per system (kg)	Systems per year	Annual precipitation ($kg\ yr^{-1}$)	Annual BL mass flux ($kg\ yr^{-1}$)
MCS's (non-TC, non-MCC)	7.06×10^4 (Max. cloud shield)	4.3 h	3.23×10^{11}	8.76×10^5	2.83×10^{17}	1.82×10^{19}
Tropical cyclones	1.40×10^6 (6° radius)	7 d	1.47×10^{14}	80	1.17×10^{16}	7.45×10^{17}
MCC's	2.25×10^5 (Max. cloud shield)	8.3 h	2.02×10^{12}	1762	3.56×10^{15}	2.29×10^{17}
Extratropical cyclones	1.40×10^6 (6° radius)	5 d	5.56×10^{13}	2338	1.30×10^{17}	2.36×10^{19}
Ordinary thunderstorms	$\sim 10^2$–10^3	0.5 h	7.50×10^8	7.52×10^7	5.64×10^{16}	6.77×10^{18}
All cloud venting systems					4.85×10^{17}	4.95×10^{19}

Machado and Rossow's (1993) tropical size distribution. However, Laing and Fritsch (1993) provide a 2-year global survey of MCC's, which represent only the larger sizes and best defined systems (from an infrared satellite perspective) of the entire MCS population. They provide information indicating that of the 358 average annual number of MCC's globally, about 303 occur from 30° S to 30° N (the larger number of annual MCC's given in Table 1 is discussed later). Assuming that this proportion of total to tropical MCC's is representative of all convective systems, we multiplied the power law MCS relation in Fig. 27 by 358/303, which gives a distribution with the same slope $(-\alpha)$ but with a $N(0)$ a factor of 1.18 larger. This provides an estimated annual size distribution for the entire globe. Using the same $V = R \times \mathrm{ATI}$ relation as given above, a global annual precipitation due to all deep convective systems (i.e., all cloud systems we are considering aside from extratropical cyclones) is estimated as 3.55×10^{17} kg, or 70% of total global precipitation.

7.2. Global precipitation by storm category

Ordinary thunderstorm precipitation

The estimated annual precipitation due to convective systems is partitioned among the size categories denoted by the asterisks in Fig. 27. The smallest size class is for all clouds with an equivalent radius of 0 to 60 km, with a mean radius of 30 km. In the infrared dataset used by Machado and Rossow (1993), individual pixels were sampled every 30 km; thus, these smallest systems are single infrared pixels colder than −28° C and surrounded by warmer pixels. We assume that the ATI-derived precipitation for this smallest class is due entirely to ordinary thunderstorms, and that all larger classes represent MCS's of one form or another, including tropical cyclones and MCC's. Thus, global precip-

Table 2
Mass flux and precipitation properties averaged over characteristic cloud system lifetimes

System type	Precip. rate ($kg\ s^{-1}$)	BL mass flux ($kg\ s^{-1}$)	q_{BL} ($kg\ kg^{-1}$)	Precipitation fraction from BL moisture	Precipitation efficiency
MCS's (non-TC, non-MCC)	2.09×10^7	1.34×10^9	0.016	0.72	0.70
Tropical cyclones	2.42×10^8	1.54×10^{10}	0.018	0.80	0.70
MCC's	6.76×10^7	4.35×10^9	0.016	0.72	0.70
Extratropical cyclones	1.29×10^8	2.33×10^{10}	0.007	0.80	0.63
Ordinary thunderstorms	4.17×10^5	5.00×10^7	0.015	0.90	0.50

itation due to ordinary thunderstorms is estimated at 5.64×10^{16} kg, with all types of MCS precipitation = 2.99×10^{17} kg (16% and 84%, respectively, of precipitation produced by all convective systems). This global precipitation estimate by ordinary thunderstorms is listed in Table 1. The characteristic ordinary thunderstorm, as described in Tables 1 and 2 is discussed below.

Tropical cyclone precipitation

Gray (1979) provides annual estimates of tropical cyclone precipitation. Based on his figures, there are an average of about 80 named tropical cyclones annually, lasting an average of 7 days each, with precipitation over a storm-centered circular area with 6°-latitude radius averaging 15 mm d^{-1}. These figures give an annual estimate of tropical cyclone precipitation of 1.17×10^{16} kg, which is 3.9% of all MCS precipitation, 3.3% of precipitation by all convective systems and 2.3% of total global precipitation.

MCC precipitation

Of the remaining MCS-related precipitation, some can be assigned to the well-defined MCC category, where a cold-topped cloud shield must remain larger than 100,000 km^2 for 6 h and be quasi-circular at its largest extent. Laing and Fritsch's (1993) 2-year global survey of MCC's provides a size distribution in increments of 100,000 km^2. Based on their data, we have reproduced their average annual MCC size distribution in a plot of log (N) vs. log (A) in Fig. 27 (bold solid line with large crosses denoting the size classes). This curve represents the best available observational information on the size distribution of MCC's.

The curve approximates a straight line from sizes 300,000 to 1,000,000 km^2. Based on less restrictive MCS climatologies than those based on the MCC definition, Machado et al. (1992) and Machado and Rossow (1993) show that the linear frequency distribution typically extends to the smallest sizes. Thus, we assume that the departure from linearity at Laing and Fritsch's smallest MCC classes (100,000 to 300,000 km^2) is due to the arbitrary size and duration limits of the MCC definition, and to the difficulty of detecting the smallest MCC's in 3-h satellite imagery. Also, we assume that the departure from linearity at the largest sizes is due to the 2-yr sampling period being insufficient for an accurate climatology of these rare events.

The straight dashed line (with circles) in Fig. 27 is the power law relation, $N(R) = N(0) \times R^{-\alpha}$, that best matches the bold observational MCC curve. The number of assumed systems larger than 300,000 km^2 matches the observed number well. The modelled number of all MCC-sized systems (> 100,000 km^2) is 2144 (the different number in Table 1 is discussed later), considerably more than the 358 annually cited by Laing and Fritsch, due to the observational problems discussed above.

This distribution was subdivided into smaller size classes of 25,000 km^2 to provide more resolution. This power law relation is shown in Fig. 27 as the short-dashed line with small pluses, and gives the same number of MCC's annually as does the curve based on 100,000 km^2 increments.

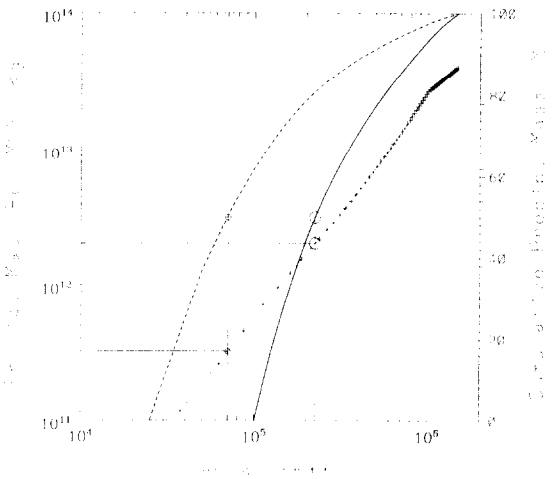

Fig. 28. Thin dashed curve is assumed MCS-total precipitation mass (left axis) as a function of maximum MCS size (abscissa), with small pluses denoting mid-points of 25,000 km^2 size classes. Bold curves are percentage cumulative annual precipitation as a function of increasing size class; solid curve is for MCC's (smallest size class beginning at 100,000 km^2), and dashed curve is for other MCS's (beginning at 25,000 km^2). The 50% cumulative volume on the MCC and MCS curves (large and small circles, respectively) identify the size and system-total precipitation of the characteristic system, as indicated.

We have also extended the power law relation down to smaller sizes (smallest class 25,000 to 50,000 km^2), in order to treat smaller than MCC-sized MCS's later. Several physical characteristics were assumed for each size class, including system duration, its growth/decay lifecycle and total precipitation per system (see Fig. 28). These size-dependent variables were based primarily on the MCC study by McAnelly and Cotton (1989). The system-total precipitation volume is modelled as $V = c \times \mathrm{ATI}^k$, where c and K are empirical constants ($k \approx 1.0$) and ATI is computed based on an assumed life-cycle. This relation follows ideas by Doneaud et al. (1984) and Griffith (1987), and well represents the system-total precipitation through the MCC size spectrum and down to the smaller MCS classes. Based on the power-law frequency distribution (Fig. 27) and the assumed size-dependent system-total precipitation (Fig. 28), total annual MCC precipitation is an estimated 3.56×10^{15} kg. This represents only 1.2%, 1.0% and 0.7% of all MCS's, all convective systems and total global precipitation, respectively.

Precipitation due to MCS's other than tropical cyclones and MCC's

After subtracting tropical cyclone and MCC precipitation from the total MCS category, the bulk (95%) of remaining MCS precipitation, 2.83×10^{17} kg, is attributed to all other kinds of MCS's. These include most squall lines, tropical cloud clusters that do not meet MCC criteria, and the multitude of convective clusters that are larger than individual cells or small multi-cell clusters. Since the Machado and Rossow (1993) size distribution provides little information on the life-cycle characteristics of MCS's, we use the MCC distribution with 25,000 km^2 size classes, extending to the smaller-than-MCC classes in Fig. 27, to also represent the size-dependent characteristics of the remaining MCS distribution (e.g., Fig. 28). To do this, we used an $N(0)$ in the power law relation such that the cumulative total precipitation for all systems larger than 25,000 km^2 was 2.83×10^{17} kg.

Extratropical cyclone precipitation

After accounting for all non-cloud-venting precipitation (5%) and all precipitation due to deep convective systems (70%), the remaining 25% of global precipitation, or 1.30×10^{17} kg, is attributed to slantwise ascent in extratropical cyclones. Note that strong cold-topped convection that occurs with extratropical cyclones, whether as ordinary thunderstorms or MCS's, have already been taken into account. Thus, we are dealing with the remaining non-convective or weak convective portions of cyclones here.

A 20-year climatology of northern hemisphere extratropical cyclogenesis and cyclone frequency, tabulated in 5° latitude/longitude blocks, was provided by Whittaker and Horn (1982). From their cyclogenesis data, we derived an annual number of Northern Hemisphere cyclones of 1169. We assume that the Southern Hemisphere produces as many, giving a total number of extratropical cyclones of 2338 per year.

7.3. Characteristic systems

In this section we discuss the characteristic storm in each category. Table 1 summarizes the size, duration and total precipitation of each characteristic storm, along with their annual frequency and total contributions to annual precipitation and mass flux from the boundary layer. Table 2 gives the precipitation and boundary layer mass flux rates, which are related through

$$V = MF \times q \times Fract^{-1} \times PE, \qquad (14)$$

where V is the precipitation mass rate, MF is the upward vertical flux of boundary layer mass through 900 mb, q is the average boundary layer mixing ratio, $Fract$ is the fraction of precipitation which is supplied by boundary layer moisture and PE is the precipitation efficiency. All of these variables are averaged over the storm lifetime. The total annual precipitation and mass flux in Table 1 are also related by the same variables. It should be emphasized that the variables (e.g., mean q) are meant to represent mean conditions throughout the year over all locations where the particular storm type occurs, and that individual cases would have large variations from these values.

Ordinary thunderstorms

As stated earlier, total precipitation due to ordinary thunderstorms was estimated by apply-

ing a simple ATI technique to the smallest size category of the entire convective system size distribution. The last four variables in Table 2 were all assumed, as was the 0.5-h active lifetime in Table 1, all based on typical values as seen in our numerical simulations. This provided a rainfall rate and storm-total rainfall for the characteristic storm. The annual total precipitation divided by the characteristic storm total gives the annual total of 7.52×10^7 ordinary thunderstorms per year. The corresponding amount of boundary layer air vented by ordinary thunderstorms per year is 6.77×10^{18} kg over the globe.

MCC's

Total annual MCC precipitation was derived from the power law MCS size distribution for 25,000 km^2 size classes in Fig. 27 and on the assumed size-dependent storm-total precipitation in Fig. 28. The characteristic MCC was defined by the size of the system in Fig. 28 that divided in half the cumulative total of annual MCC precipitation. This characteristic MCC has a maximum cloud shield ($-33°$ C threshold) of 225,000 km^2, meets MCC size-criteria for 8.3 h, and produces 2.02×10^{12} kg of precipitation, all of which are smaller than values for the average system described by McAnelly and Cotton (1989) and Laing and Fritsch (1993). The smaller characteristic MCC results from assuming the power law relation to the smallest MCC sizes (Fig. 27). Note that the annual number of MCC's in Table 1 (1762) is given by annual MCC precipitation divided by the characteristic storm total, and differs from the 2144 cited in the third part of Section 7.2. The precipitation rate in Table 2 is the characteristic storm total divided by lifetime, and the last three variables in Table 2 were assumed. The lower value of 0.72 for *Fract* (relative to the other storm types) is related to the in-situ growth of hydrometeors in mesoscale ascent within the stratiform region of MCC's, which is partially fed by moisture convergence from air well above the boundary layer. The resultant annual precipitation by MCC's is estimated to be 3.56×10^{15} kg and the amount of boundary layer air vented is 2.29×10^{17} kg, which is less than that vented by ordinary thunderstorms.

Other MCS's

The characteristic MCS was derived in the same manner as was the characteristic MCC, except we extended the MCC power law relation in Fig. 27 to smaller-than-MCC size classes. The inclusion of these smaller classes dominates the cumulative precipitation curve in Fig. 28 and results in a characteristic MCS that is about a third the size of the typical MCC. The large annual number of these relatively small MCS's, compared to the relatively few larger MCC's, is quite realistic. The resultant estimated total precipitation from MCS's (excluding tropical cyclones and MCC's) is 2.83×10^{17} kg and the corresponding boundary layer mass transported by them per year is 1.82×10^{19} kg; two orders of magnitude greater than for the MCC class. The combined total boundary layer mass transport by all MCS's including MCC's is roughly 1.84×10^{19} kg.

Tropical cyclones

The figures provided by Gray (1979), discussed above, provide the annual precipitation contribution of tropical cyclones and dimensions of the typical system in Table 1, along with its volumetric precipitation rate in Table 2. The last three variables in Table 2 were all assumed, and the mass flux was computed. The total annual precipitation estimated is 1.17×10^{16} kg and the total global annual boundary layer air transported by tropical cyclones is 7.45×10^{17} kg. The values in Table 2 agree fairly well with the RAMS simulations described in Section 5, when one takes into account that the 400×400 km domain represents only the innermost 2° of the entire 6° radius considered by Gray (1979). In fact, the 40–45% of total storm precipitation shown by Gray to occur in the inner 2° radius matches that of the RAMS simulation very closely. The values in Table 2 are also quite consistent with those derived (for a smaller core region) in the observational case study by Riehl and Malkus (1961).

Extratropical cyclones

The annual number and total annual precipitation of extratropical cyclones was given as described above. Division of total precipitation by number of systems gives 5.56×10^{13} kg per sys-

tem in Table 1, and the assumed average duration of 5 days gives the average precipitation rate in Table 2. This yields an estimated total nonconvective contribution to the annual precipitation from extratropical cyclones of 1.30×10^{17} kg. The upward mass flux through 900 mb in Table 2 was based on an average of (and inferences from) case studies, analytical models, and numerical simulations of extratropical cyclones by Palmen and Newton (1969), Sanders (1971), Bosart and Lin (1984), Nuss and Anthes (1987), and Wash et al. (1988). With the assumed values of q and *Fract* in Table 2, precipitation efficiency was calculated at 0.63, which seems reasonable. Thus the slantwise ascending motions in extratropical cyclones transport 2.36×10^{19} kg of boundary layer air annually, which exceeds the amount transported by any other storm type we have considered.

8. Summary and conclusions

In this paper we have reviewed observational and modeling studies of cloud venting by a wide variety of cloud types ranging from ordinary cumuli, to ordinary cumulonimbi, mesoscale convective systems, and tropical and extratropical cyclones. We have also run explicit cloud-resolving simulations using RAMS to illustrate the nature of boundary layer venting by several cloud system types and to provide quantitative estimates of the transport rates for the different storms. It is shown that the amounts of boundary layer air vented varies considerably depending on storm system type. Even within the broad class of cumulonimbi (excluding MCS's), there is considerable variability in the amount of boundary layer air vented. A supercell thunderstorm, for example, can transport some 12 times more boundary layer air over its lifetime than a single ordinary cumulonimbus.

MCS's, which are comprised of both deep convective updrafts and slowly ascending mesoscale flow branches, can vent more than 40 times the mass of boundary layer air as supercell thunderstorms. The simulations with RAMS, however, revealed that the slantwise ascending branches of MCS's do not directly access boundary layer air (i.e., MCC's) and do not directly participate in venting of boundary layer air. In combination with ordinary cumuli which may vent boundary layer air up to 3 to 5 km levels prior to the formation of an MCS, these slantwise branches, however, can contribute to substantial venting of the boundary layer.

We have also attempted to make global annual estimates of the contributions of the various storm types to venting of boundary layer air. Based on Table 2, we see that the characteristic extratropical cyclone has the highest boundary layer mass flux of all deep cloud venting systems, followed by tropical cyclones, MCC's, other MCS's, and finally ordinary thunderstorms. This hierarchy is intuitive based on the scales of the storm types. In terms of annual mass flux in Table 1, extratropical cyclones still contribute the most. The great numbers of MCS's and ordinary thunderstorms, however, result in those classes being second and third in annual contribution to total boundary layer air vented, followed by tropical cyclones and MCC's. The total annual flux of 4.95×10^{19} kg of boundary layer air by these cloud systems represents a venting of the entire planetary boundary layer about 90 times a year.

In view of our estimate of the dominance of extratropical cyclones to the global annual venting of boundary layer air, it is important that climate models either explicitly resolve these weather systems or parameterize their transport characteristics properly. Likewise, because MCS's are a major contributor to venting boundary layer air, especially at low latitudes, an effort should be made to accurately parameterize those storms in climate models.

Acknowledgements

Brenda Thompson is acknowledged for her contribution to processing the manuscript prepared by a number of authors. Original research in this article was supported in part by the Department of Energy under contracts DE-FG02-90ER61066 and DE-FG03-94ER61749. Financial support does not constitute an endorsement by

DOE of the views expressed in this article. This research was also supported in part by the National Science Foundation under grant ATM-9118963.

References

Alheit, R.R. and Hauf, T., 1992. Vertical transport of trace species by thunderstorms — A transilient transport model. Ber. Bunsenges. Phys. Chem., 96: 501–510.

Asai, T. and Kasahara, A., 1967. A theoretical study of the compensating downward motions associated with cumulus clouds. J. Atmos. Sci., 24: 487–497.

Banic, C.M., Isaac, G.A., Cho, H.R. and Iribarne, J.V., 1986. The distribution of pollutants near a frontal surface: A comparison between field experiment and modeling. Water, Air Soil Pollut., 30: 171–177.

Barth, M.C., Hegg, D.A. and Hobbs, P.V., 1992. Numerical modeling of cloud and precipitation chemistry associated with two rainbands and some comparisons with observations. J. Geophys. Res., 97: 5825–5845.

Blyth, A.M. and Latham, J., 1985. An airborne study of vertical structure and microphysical variability within a small cumulus. Q. J. R. Meteorol. Soc., 111: 773–792.

Boatman, J.F. and Auer, A.H., 1983. The role of cloud top entrainment in cumulus clouds. J. Atmos. Sci., 40: 1517–1534.

Bosart, L.F. and Lin, S.C., 1984. A diagnostic analysis of the Presidents' Day Storm of February 1979. Mon. Weather Rev., 112: 2148–2177.

Bosart, L.F. and Sanders, F., 1981. The Johnstown Flood of July 1977: A long-lived convective system. J. Atmos. Sci., 38: 1616–1642.

Braham, R.R., 1952. The water and energy budgets of the thunderstorm and their relation to thunderstorm development. J. Meteorol., 9: 227–242.

Brost, R.A., Chatfield, R.B., Greenberg, J., Haagenson, P.L., Heikes, B.G., Madronich, S., Ridley, B. and Zimmerman, P.R., 1988. Three-dimensional modeling of transport of chemical species from continents to the Atlantic Ocean. Tellus, 40B: 358–379.

Browning, K.A., 1993. The GEWEX Cloud System Study (GCSS). Bull. Am. Meteorol. Soc., 74: 387–399.

Carlson, T.N., 1980. Airflow through midlatitude cyclones and the comma cloud pattern. Mon. Weather Rev., 108: 1498–1509.

Chang, J.S., Brost, R.A., Isaksen, I.S.A., Madronich, S., Middleton, P., Stockwell, W.R. and Walcek, C.J., 1987. A three-dimensional Eulerian acid deposition model: Physical concepts and fromulation. J. Geophys. Res., 92: 14,681–14,700.

Chatfield, R.B. and Crutzen, P.J., 1984. Sulfur dioxide in remote oceanic air: Cloud transport of reactive precursors. J. Geophys. Res., 89: 7111–7132.

Chatfield, R.B. and Delany, A.C., 1990. Convection links biomass burning to increased tropical ozone: However, models will tend to overpredict O_3. J. Geophys. Res., 95 18,473–18,488.

Chatfield, R.B., Gardner, E.P. and Calvert, J.G., 1987. Sources and sinks of acetone in the troposphere: Behavior of reactive hydrocarbons and a stable product. J. Geophys. Res., 92: 4208–4216.

Chaumerliac, N., Rosset, R., Renard, M. and Nickerson, E.C., 1992. The transport and redistribution of atmospheric gases in regions of frontal rain. J. Atmos. Chem., 14: 43–51.

Ching, J., 1982. The role of convective clouds in venting ozone from the mixed layer. Preprints, 3rd Joint Conf. Applications of Air Pollution Meteorology, 12–15 Jan 1982, San Antonio, Am. Meteorol. Soc.

Ching, J.K.S., 1989. Simulating vertical transport and transformation of mixed layer pollutants by non-precipitating convective cumulus clouds. Preprints, 6th Conf. Applications of Air Pollution Meteorology, 30 Jan.–3 Feb. 1989, Anaheim, CA, Am. Meteorol. Soc., pp. J19–J22.

Ching, J.K.S. and Alkezweeny, A.J., 1986. Tracer study of vertical exchange by cumulus clouds. J. Climate Appl. Meteorol., 25: 1702–1711.

Ching, J.K.S., Shipley, S.T. and Browell, E.V., 1988. Evidence for cloud venting of mixed layer ozone and aerosols. Atmos. Environ., 22: 225–242.

Cho, H.-R., Iribarne, J.V., Grabenstetter, J.E. and Tam, Y.T., 1983. Effects of cumulus cloud systems on the vertical distribution of air pollution. Trans. Meteorol. Acid Dep., APCP, pp. 127–139.

Cho, H.-R., Iribarne, J.V., Kavassalis, T.A., Melo, O.T., Tam, Y.T. and Moroz, W.J., 1986. Effect of a stratus cloud on the redistribution and transformation of pollutants. Water, Air Soil Pollut., 30: 195–203.

Cho, H.R., Niewiandomski, M. and Iribarne, J.V., 1989. A model of the effect of cumulus clouds on the redistribution and transformation of pollutants. J. Geophys. Res., 94: 1895–1910.

Clark, T.L., 1977. A small-scale dynamic model using a terrain-following coordinate transformation. J. Comput. Phys., 24: 186–215.

Clark, T.L., 1979. Numerical simulations with a three-dimensional cloud model: Lateral boundary condition experiments and multicellular storm simulations. J. Atmos. Sci., 36: 2191–2215.

Clark, T.L. and Farley, R.D., 1984. Severe downslope windstorm calculations in two and three spatial dimensions using anelastic interactive grid nesting: A possible mechanism for gustiness. J. Atmos. Sci., 41: 329–350.

Cotton, W.R., 1975. On parameterization of turbulent transport in cumulus clouds. J. Atmos. Sci., 32: 548–564.

Cotton, W.R. and Anthes, R.A., 1989. Storm and Cloud Dynamics. Academic Press, San Diego. International Geophysics Series, Vol. 44., 883 pp.

Cram, J.M., Pielke, R.A. and Cotton, W.R., 1992a. Numerical simulation and analysis of a prefrontal squall line. Part I:

Observations and basic simulation results. J. Atmos. Sci., 49: 189–208.

Cram, J.M., Pielke, R.A. and Cotton, W.R., 1992b. Numerical simulation and analysis of a prefrontal squall line. Part II: Propagation of the squall line as an internal gravity wave. J. Atmos. Sci., 49: 209–225.

Cunning, J.B., 1986. The Oklahoma–Kansas Preliminary Regional Experiment for STORM Central. Bull. Am. Meteorol. Soc., 67: 1478–1486.

Dickerson, R.R., Huffman, G.J., Luke, W.T., Nunnermacker, L.J., Pickering, K.E., Leslie, A.C.D., Lindsey, C.G., Slinn, W.G.N., Kelly, T.J., Daum, P.H., Delany, A.C., Greenberg, J.P., Zimmerman, P.R., Boatman, J.F., Ray, J.D. and Stedman, D.H., 1987. Thunderstorms: An important mechanism in the transport of air pollutants. Science, 235: 460–465.

Doneaud, A.A., Ionescu-Niscov, S., Priegnitz, D.L. and Smith, P.L., 1984. The area–time integral as an indicator for convective rain volumes. J. Climate Appl. Meteorol., 23: 555–561.

Dye, J.E., Jones, J.J., Winn, W.P., Cerni, T.A., Gardiner, B., Lamb, D., Pitter, R.L., Hallet, J. and Saunders, C.P.R., 1986. Early electrification and precipitation development in a small isolated Montana cumulonibus. J. Geophys. Res., 91: 1231–1247.

Fishman, J. and Larsen, J.C., 1987. The distribution of total ozone, stratospheric ozone, and tropospheric ozone at low latitudes deduced from satellite data sets. In: R. Bijkov and P. Fabian (Editors), Ozone in the Atmosphere. Deepak, Hampton, VA, pp. 411–414.

Flossman, A.I., 1991. The scavenging of two different types of marine aerosol particles calculated using a two-dimensional detailed cloud model. Tellus, 43B: 301–321.

Flossman, A.I., 1993. The effect of the impaction scavenging efficiency on the wet deposition by a convective warm cloud. Tellus, 45B: 34–39.

Flossman, A.I. and Pruppacher, H.R., 1988. A theoretical study of the wet removal of atmospheric pollutants. Part III: The uptake, redistribution, and deposition of $(NH_4)_2SO_4$ particles by a convective cloud using a two-dimensional cloud dynamics model. J. Atmos. Sci., 45: 1857–1871.

Fortune, M.A., 1989. The Evolution of Vortical Patterns and Vortices in Mesoscale Convective Complexes. Ph.D. Diss., Colorado State Univ. Dep. Atmospheric Science, Fort Collins, CO 80523.

Garstang, M., Scala, J., Greco, S., Harriss, R., Beck, S., Browell, E., Sachse, G., Gregory, G., Hill, G., Simpson, J., Tao, W.-K. and Torres, A., 1988. Trace gas exchanges and convective transports over the Amazonian rain forest. J. Geophys. Res., 93: 1528–1550.

Goodman, S.J. and MacGorman, D.R., 1986. Cloud-to-ground lightning activity in mesoscale convective complexes. Mon. Weather Rev., 114: 2320–2328.

Grasso, L.D., 1992. A Numerical Simulation of Tornadogenesis. Atmos. Sci. Pap., 495, Colorado State Univ., Dep. Atmospheric Science, Fort Collins, CO 80523, 102 pp.

Gray, W.M., 1979. Hurricanes: their formation, structure and likely role in the tropical circulation. In: Shaw (Editor), Meteorology over the Tropical Oceans. R. Meteorol. Soc., pp. 155–218.

Gray, W.M., Ruprecht, E. and Phelps, R., 1975. Relative humidity in tropical weather systems. Mon. Weather Rev., 103: 685–690.

Greenhut, G.K., 1986. Transport of ozone between boundary layer and cloud layer by cumulus clouds. J. Geophys. Res., 91: 8613–8622.

Griffith, C.G., 1987. Comparisons of gauge and satellite rain estimates for the central United States during August 1979. J. Geophys. Res., 92: 9551–9566.

Hall, W.D., 1980. A detailed microphysical model within a two-dimensional dynamic framework: Model description and preliminary results. J. Atmos. Sci., 37: 2486–2507

Hegg, D.A., Rutledge, S.A. and Hobbs, P.V., 1984. A numerical model for sulfur chemistry in warm-frontal rainbands. J. Geophys. Res., 89: 7133–7147.

Hegg, D.A., Rutledge, S.A. and Hobbs, P.V., 1986. A numerical model for sulfur and nitrogen scavenging in narrow cold-frontal rainbands. 2. Discussion of chemical fields. J. Geophys. Res., 91: 14,403–14,416.

Hertenstein, R.F.A., Cotton, W.R. and Weissbluth, M.J., 1992. Quasi-three-dimensional simulations of deep convection. Preprints, 5th Conf. Mesoscale Processes, 5–10 Jan. 1992, Atlanta, GA, Am. Meteorol. Soc., pp. 381–384.

Heymsfield, A.J., Johnson, D.N. and Dye, J.E., 1978. Observations of moist adiabatic ascent in northeast Colorado cumulus congestus clouds. J. Atmos. Sci., 35: 1689–1703.

Heymsfield, A.J. and Miller, K.M., 1988. Water vapor and ice mass transported into the anvils of CCOPE thunderstorms: Comparison with storm influx and rainout. J. Atmos. Sci., 45, 3501–3514.

Hoppel, W.A., Frick, G.M. and Larson, R.E., 1986. Effect of nonprecipitating clouds on the aerosol size distribution in the marine boundary layer. Geophys. Res. Lett., 13: 125–128.

Hoskins, B.J. and Bretherton, F.P., 1972. Atmospheric frontogenesis models: Mathematical formulation and solution. J. Atmos. Sci., 29: 11–37.

Houze, R.A., Jr. and Hobbs, P.V., 1982. Organization and structure of precipitating cloud systems. Adv. Geophys., 24. Academic Press, New York, pp. 225–315.

Isaac, G.A., P.I. Joe and P.W. Summers, 1983. The vertical transport and redistribution of pollutants by clouds. Transactions, Specialty Conf. on the Meteorology of Acid Deposition, October 1983, Air Pollut. Control Assoc., 496–512.

Isaac, G.A., Strapp, J.W., Schemenauer, R.S. and MacPherson, J.I., 1982. Summer cumulus cloud seeding experiments near Yellowknife and Thunder Bay, Canada. J. Appl. Meteorol., 21: 1266–1285.

Janowiak, J.E., 1992. Tropical rainfall: A comparison of satellite-derived rainfall estimates with model precipitation forecasts, climatologies, and observations. Mon. Weather Rev., 120: 448–462.

Jensen, J.B., Austin, P.H., Baker, M.B. and Blyth, A.M., 1985.

Turbulent mixing, spectral evolution and dynamics in a warm cumulus cloud. J. Atmos. Sci., 42: 173–192.

Johnson, R.H. and Hamilton, P.J., 1988. The relationship of surface pressure features to the precipitation and air flow structure of an intense midlatitude squall line. Mon. Weather Rev., 116: 1444–1472.

Jordan, C.L., 1958. Mean soundings for the West Indies area. J. Meteorol., 15: 91–97.

Kavassalis, T.A., Melo, O.T., Iribarne, J.V. and Cho, H.-R., 1986. Cloud microphysics and acid rain formation in frontal circulations. In: J. Laznow and G.J. Stensland (Editors), Preprints, 2nd Int. Speciality Conf. Meteorology of Acidic Deposition. Air Pollution Control Assoc., pp. 278–301.

Kitada, T., Lee, P.C.S. and Ueda, H., 1993. Numerical modeling of long-range transport of acidic species in associated with meso-β convective clouds across the Japan Sea resulting in acid snow over coastal Japan — 1. Model description and qualitative verifications. Atmos. Environ., 27A: 1061–1076.

Kitada, T. and Lee, P.C.S., 1993. Numerical modeling of long-range transport of acidic species in association with meso-β convective clouds across the Japan Sea resulting in acid snow over coastal Japan — II. Results and discussion. Atmos. Environ., 27A: 1077–1090.

Knupp, K.R., 1985. Precipitation Convective Downdraft Structure: A Synthesis of Observations and Modeling. Ph.D. Diss. Colorado State Univ. Dep. Atmospheric Science, Fort Collins, CO 80523.

Lafore, J.-P. and Moncrieff, M.W., 1989. A numerical investigation of the organization and interaction of the convective and stratiform regions of tropical squall lines. J. Atmos. Sci., 46: 521–544.

Laing, A. and Fritsch, J.M., 1993. Mesoscale convective complexes in Africa. Mon. Weather Rev., 121: 2254–2263.

Leaitch, W.R., Strapp, J.W., Wiebe, H.A. and Isaac, G.A., 1982. Measurements of scavenging and transformation of aerosols inside cumulus. In: H.R. Pruppacher, R.G. Semonin and W.G.N. Slinn (Coordinators), Precipitation Scavenging, Dry Deposition and Resuspension. Elsevier, Amsterdam, pp. 53–69.

Lee, In-Y., 1986. Numerical simulation of chemical and physical properties of cumulus clouds. Atmos. Environ., 20: 767–771.

Lyons, W.A., Calby, R.H. and Keen, C.S., 1986. The impact of mesoscale convective systems on regional visibility and oxidant distribution during persistent elevated pollution episodes. J. Clim. Appl. Meteorol., 25: 1518–1531.

Machado, L.A.T., Desbois, M. and Duvel, J.-P., 1992. Structural characteristics of deep convective systems over tropical Africa and Atlantic Ocean. Mon. Weather Rev., 120: 392–406.

Machado, L.A.T., Duvel, J.-P. and Desbois, M., 1993. Diurnal variations and modulation by easterly waves of the size distribution of convective cloud clusters over West Africa and the Atlantic Ocean. Mon. Weather Rev., 121: 37–49.

Machado, L.A.T. and Rossow, W.B., 1993. Structural characteristics and radiative properties of tropical cloud clusters. Mon. Weather Rev., 121: 3234–3260.

Maddox, R.A., 1980. Mesoscale convective complexes. Bull. Am. Meteorol. Soc., 61: 1374–1387.

Marwitz, J.D., 1972a. The structure and motion of severe hailstorms. Part I: Supercell storms. J. Appl. Meteorol., 11: 166–179.

Marwitz, J.D., 1972b. The structure and motion of severe hailstorms. Part II: Multicell storms. J. Appl. Meteorol., 11: 180–188.

Marwitz, J.D., 1972c. The structure and motion of severe hailstorms. Part III: Severely sheared storms. J. Appl. Meteorol., 11: 189–201.

McAnelly, R.L. and Cotton, W.R., 1989. The precipitation life cycle of mesoscale convective complexes over the central United States. Mon. Weather Rev., 117: 784–808.

Mitra, S.K., Pruppacher, H.R. and Brinkmann, J., 1992. A wind tunnel study on the drop-to particle conversion. J. Aerosol Sci., 23: 245–256.

Moncrieff, M.W. and Green, J.S.A., 1972. The propagation and transfer properties of steady convective overturning in shear. Q. J. R. Meteorol. Soc., 98: 336–352.

Nicholls, M.E. and Weissbluth, M.J., 1988. A comparison of two-dimensional and quasi-three-dimensional simulations of a tropical squall line. Mon. Weather Rev., 116: 2437–2452.

Niewiadomski, M., 1986. A passive pollutant in a three-dimensional field of convective clouds: Numerical simulations. Atmos. Environ., 20: 139–145.

Niewiadomski, M., Kavassalis, T.A. and Melo, O.T., 1986. A one-dimensional, two-stream model of transport of pollutants and liquid water acidification in cumulus clouds. Trans. Meteorol. Acid Dep. APCA, pp. 238–256.

Nuss, W.A. and Anthes, R.A., 1987. A numerical investigation of low-level processes in rapid cyclogenesis. Mon. Weather Rev., 115: 2728–2743.

Pakiam, J.E. and Maybank, J., 1975. The electrical characteristics of some severe hailstorms in Alberta, Canada. J. Meteorol. Soc. Jpn., 53: 363–383.

Palmen, E. and Newton, C.W., 1969. Atmospheric Circulation Systems: Their Structure and Physical Interpretation. International Geophysics Series, Vol. 13. Academic Press, New York, 603 pp.

Paluch, I.R., 1979. The entrainment mechanism in Colorado cumuli. J. Atmos. Sci., 36: 2462–2478.

Pickering, K.E., Dickerson, R.R., Luke, W.T. and Nunnermacker, L.J., 1989. Clear sky vertical profiles of trace gases as influenced by upstream convective activity. J. Geophys. Res., 94: 14,879–14,892.

Pickering, K.E., Thompson, A.M., Dickerson, R.R., Luke, W.T., McNamara, D.P., Greenberg, J.P. and Zimmerman, P.R., 1990. Model calculations of tropospheric ozone production potential following observed convective events. J. Geophys. Res., 95: 14,049–14,062.

Pickering, K.E., Thompson, A.M., Scala, J.R., Tao, W-K., Simpson, J. and Garstang, M., 1991. Photochemical ozone production in tropical squall line convection during NASA Global Tropospheric Experiment/Amazon Boundary Layer Experiment 2A. J. Geophys. Res., 96: 3099–3114.

Pielke, R.A., Cotton, W.R., Walko, R.L., Tremback, C.J., Lyons, W.A., Grasso, L.D., Nicholls, M.E., Moran, M.D., Wesley, D.A., Lee, T.J. and Copeland, J.H., 1992. A comprehensive meteorological modeling system — RAMS. Meteorol. Atmos. Phys., 49: 69–91.

Ray, P.S., Johnson, B.C., Johnson, K.W., Bradberry, J.S., Stephens, J.J., Wagner, K.K., Wilhelmson, R.B. and Klemp, J.B., 1981. The morphology of several tornadic storms 20 May 1977. J. Atmos. Sci., 38: 1643–1663.

Riehl, H., 1979. Climate and Weather in the Tropics. Academic Press, London, 611 pp.

Riehl, H. and Malkus, J.S., 1958. On the heat balance in the equitorial trough zone. Geophysica, 6: 503–538.

Riehl, H. and Malkus, J., 1961. Some aspects of Hurricane Daisy, 1958. Tellus, 13: 181–213.

Rutledge, S.A., Hegg, D.A. and Hobbs, P.V., 1986. A numerical model for sulfur and nitrogen scavenging in narrow cold-frontal rainbands. 1. Model description and discussion of microphysical fields. J. Geophys. Res., 91: 14,385–14,402.

Rutledge, S.A. and Hobbs, P.V., 1983. The mesoscale and microscale structure and organization of clouds and precipitation in midlatitude cyclones. VIII: A model for the "seeder-feeder" process in warm-frontal rainbands. J. Atmos. Sci., 40: 1185–1206.

Sanders, F., 1971. Analytic solutions of the nonlinear omega and vorticity equations for a structurally simple model of disturbances in the baroclinic westerlies. Mon. Weather Rev., 99: 393–407.

Sanders, F. and Gyakum, J.R., 1980. Synoptic-dynamic climatology of the "bomb." Mon. Weather Rev., 108: 1589–1606.

Scala, J.R., Garstang, M., Tao, W.-K., Pickering, K.E., Thompson, A.M., Simpson, J., Kirchhoff, V.W.J.H., Browell, E.V., Sachse, G.W., Torres, A.L., Gregory, G.L., Rasmussen, R.A. and Khalil, M.A.K., 1990. Cloud draft structure and trace gas transport. J. Geophys. Res., 95: 17,015–17,030.

Smolarkiewicz, P.K. and Clark, T.L., 1985. Numerical simulation of the evolution of a three-dimensional field of cumulus clouds. Part I: Model description, comparison with observations and sensitivity studies. J. Atmos. Sci., 42: 502–522.

Staley, D.O. and Gall, R.L., 1977. On the wavelength of maximum baroclinic instability. J. Atmos. Sci., 34: 1679–1688.

Stormfury, 1970. Project Stormfury Annual Report 1969, National Hurricane Research Laboratory, NOAA, Coral Gables, FL, 20 pp.

Stull, R.B., 1985. A fair-weather cumulus cloud classification scheme for mixed-layer studies. J. Climate Appl. Meteorol., 24: 49–56.

Stull, R.B. and Eloranta, E.W., 1984. Boundary Layer Experiment, 1983. Bull. Am. Meteorol. Soc., 65: 450–456.

Taylor, G.R., 1989a. Sulfate production and deposition in midlatitude continental cumulus clouds. Part I: Cloud model formulation and base run analysis. J. Atmos. Sci., 46: 1971–1990.

Taylor, G.R., 1989b. Sulfate production and deposition in midlatitude continental cumulus clouds. Part II: Chemistry model formulation and sensitivity analysis. J. Atmos. Sci., 46: 1991–2007.

Tremblay, A. and Leighton, H., 1986. A three-dimensional cloud chemistry model. J. Clim. Appl. Meteorol., 25: 652–671.

Tripoli, G. and Cotton, W.R., 1989a. A numerical study of an observed orogenic mesoscale convective system. Part 1. Simulated genesis and comparison with observations. Mon. Weather Rev., 117: 273–304.

Tripoli, G. and Cotton, W.R., 1989b. A numerical study of an observed orogenic mesoscale convective system. Part 2. Analysis of governing dynamics. Mon. Weather Rev., 117: 305–328.

Verlinde, J. and Cotton, W.R., 1990. A critical look at kinematic microphysical retrieval algorithms. Proc. Conf. Cloud Physics, July 23–27, 1990, San Francisco, CA.

Verlinde, J. and Cotton, W.R., 1993. Fitting microphysical observations of non-steady convective clouds to a numerical model: An application of the adjoint technique of data assimilation to a kinematic model. Mon. Weather Rev., 121: 2776–2793.

Vukovich, F.M. and Ching, J.K.S., 1990. A semi-empirical approach to estimate vertical transport by nonprecipitating convective clouds on a regional scale. Atmos. Environ., 24A: 2153–2168.

Walcek, C.J., Stockwell, W.R. and Chang, J.S., 1990. Theoretical estimates of the dynamic, radiative and chemical effects of clouds on tropospheric trace gases. Atmos. Res., 25: 53–69.

Walcek, C.J. and Taylor, G.R., 1986. A theoretical method for computing vertical distribution of acidity and sulfate production within cumulus clouds. J. Atmos. Sci., 43: 339–355.

Walko, R.L., Cotton, W.R. and Pielke, R.A., 1992. Large eddy simulations of the effects of hilly terrain on the convective boundary layer. Boundary-Layer Meteorol., 53: 133–150.

Wang, C. and Chang, J.S., 1993a. A three-dimensional numerical model of cloud dynamics, microphysics, and chemistry. 1. Concepts and formulation. J. Geophys. Res., 98: 14,827–14,844.

Wang, C. and Chang, J.S., 1993b. A three-dimensional numerical model of cloud dynamics, microphysics, and chemistry. 2. A case study of the dynamics and microphysics of a severe local storm. J. Geophys. Res., 98: 14,845–14,862.

Wang, C. and Chang, J.S., 1993c. A three-dimensional numerical model of cloud dynamics, microphysics, and chemistry. 3. Redistribution of pollutants. J. Geophys. Res., 98: 16,787–16,798.

Wang, C. and J.S. Chang, 1993d. A three-dimensional numerical model of cloud dynamics, microphysics, and chemistry. 4. Cloud chemistry and precipitation chemistry. J. Geophys. Res., 98: 16,799–16,808.

Warner, J., 1970. The microstructure of cumulus cloud. Part III. The nature of the updraft. J. Atmos. Sci., 27: 682–688.

Wash, C.H., Peak, J.E., Calland, W.E. and Cook, W.A., 1988. Diagnostic study of explosive cyclogenesis during FGGE. Mon. Weather Rev., 116: 431–451.

Weisman, M.L. and Klemp, J.B., 1984. The structure and classification of numerically simulated convective storms in directionally varying wind shears. Mon. Weather Rev., 112: 2479–2498.

Wetzel, P.J., Cotton, W.R. and McAnelly, R.L., 1983. A long-lived mesoscale convective complex. Part II: Evolution and structure of the mature complex. Mon. Weather Rev., 111: 1919–1937.

Whittaker, L.M. and Horn, L.H., 1982. Atlas of Northern Hemisphere Extratropical Cyclone Activity, 1958–1977. Dep. Meteorol. Univ. Wisconsin, 1225 W. Dayton St., Madison, WI 53706, 65 pp.

Williams, E.R., Rutledge, S.A., Feotis, S.G., Renno, N., Rasmussen, E. and Rickenbach, T., 1992. A radar and electrical study of tropical "hot" towers. J. Atmos. Sci., 49: 1386–1395.

Yau, M.K., 1980. A two-cylinder model of cumulus cells and its application in computing cumulus transports. J. Atmos. Sci., 37: 488–494.

Yau, M.K. and Michaud, R., 1982. Numerical simulation of a cumulus ensemble in three dimensions. J. Atmos. Sci., 39: 1062–1079.

William R. Cotton is a professor of atmospheric science at Colorado State University. He received his B.S. and M.S. in mathematics and atmospheric science, respectively, from the State University of New York at Albany and his Ph.D. degree in meteorology from The Pennsylvania State University. Dr. Cotton is one of the leading researchers in storm research having published over 200 technical articles and 10 books. He specializes in both computer simulation of storms, and field observation and data analysis of storm systems. He is a Fellow of the American Meteorological Society.